scRNAseq unravels the transcriptional network underlying zebrafish retina regeneration

Laura Celotto[1], Fabian Rost[2], Anja Machate[1], Juliane Bläsche[2], Andreas Dahl[2], Anke Weber[1], Stefan Hans[1], and Michael Brand[*1]

[1] Technische Universität Dresden, CRTD - Center for Regenerative Therapies Dresden, Center for Molecular and Cellular Bioengineering (CMCB), Fetscherstraße 105, 01307 Dresden, Germany

[2] Technische Universität Dresden, DRESDEN-Concept Genome Center, Center for Molecular and Cellular Bioengineering (CMCB), Fetscherstraße 105, 01307 Dresden, Germany

*Corresponding author

ORCID: Laura Celotto: 0000-0002-9191-4056; Fabian Rost: 0000-0001-6466-2589; Andreas Dahl: 0000-0002-2668-8371; Anke Weber: 0000-0003-2220-658X; Stefan Hans: 0000-0003-0283-0211; Michael Brand: 0000-0001-5711-6512

Keywords: Retina, regeneration, zebrafish, Müller glia, progenitors, light lesion, scRNAseq

SUMMARY

In the lesioned zebrafish retina, Müller glia produce multipotent retinal progenitors that generate all retinal neurons, replacing lost cell types. To study the molecular mechanisms linking Müller glia reactivity to progenitor production and neuronal differentiation, we used single cell RNA sequencing of Müller glia, progenitors and regenerated progeny from uninjured and light-lesioned retinae. We discover an injury-induced Müller glia differentiation trajectory that leads into a cell population with a hybrid identity expressing marker genes of Müller glia and progenitors. A glial self-renewal and a neurogenic trajectory depart from the hybrid cell population. We further observe that neurogenic progenitors progressively differentiate to generate retinal ganglion cells first and bipolar cells last, similar to the events observed during retinal development. Our work provides a comprehensive description of Müller glia and progenitor transcriptional changes and fate decisions in the regenerating retina, which are key to tailor cell differentiation and replacement therapies for retinal dystrophies in humans.

INTRODUCTION

The vertebrate retina is the neural tissue in the back of the eyes that detects and processes visual stimuli prior to transmission to the brain [1]. The retina has a layered structure, with outer, inner and ganglion cell nuclear layers alternating with the outer and inner plexiform layers [2–4]. The nuclear layers comprise the nuclei of retinal neurons, whereas the plexiform layers contain neuronal synapses. There are six distinct classes of retinal neurons and one main type of glia: retinal ganglion, cone photoreceptor, horizontal, amacrine, rod photoreceptor and bipolar cells, as well as Müller glia. This heterogeneity arises during development in the indicated order from a

common pool of multipotent retinal progenitor cells (RPCs), which progressively restrict their competence to generate early and mid-late born cell fates [2,4–13]. Retinal development, structure and function are highly conserved among vertebrates, including the teleost zebrafish (*Danio rerio*) with only slight variations. For instance, humans and zebrafish possess a cone-dominated retina adapted for diurnal visual tasks, whereas nocturnal animals, like mice and rats, have rod-dominated retinae adapted for a dim light lifestyle [10,14,15]. Intriguingly, and in contrast to warm-blooded vertebrates like birds and mammals, adult zebrafish can fully regenerate their retinae upon lesions affecting different neuronal cell types, depending on the injury paradigm. For instance, intense light ablates preferentially light-sensing rod and cone photoreceptors in the central and dorsal retina, whereas application of neurotoxins, like ouabain or NMDA, affects mainly retinal ganglion and amacrine cells [16–22]. Independently of the lesion type, Müller glia (MG), acting as resident stem cells, are the primary cellular origin of regenerated cells. Specifically, zebrafish MG react to the lesion by partial dedifferentiation and cell cycle re-entry, followed by an asymmetric division producing renewed MG and multipotent RPCs [23–26]. Dedifferentiation of MG to a progenitor-like state is not complete, as MG upregulate progenitor-associated genes like *pax6* or *vsx2*, but retain their glial morphology. In this context, glial markers like Glial Fibrillary Acidic Protein (*gfap*) as well as glutamine synthase (*glula*) have been reported to be either retained or downregulated, depending on the lesion paradigm, the regeneration time point, the antibody and the transgenic line used to label MG [17,25,27,28]. However, in all reported cases, MG-derived RPCs do not express *gfap* [25,28]. Asymmetric cell division of MG occurs between 31 hours and 2 days post-lesion, followed by further proliferation of MG-derived RPCs that peaks at 4-5 days post lesion, depending on the injury paradigm [16,17,27,29]. Studies on zebrafish retina regeneration have so far mainly focused on very early phases of MG dedifferentiation

76 and RPC production [28,30–36]. Recent work showed that MG initially assume a reactive
77 state, characterized by the expression of *hmga1a* and *yap1*, prior to giving rise to
78 proliferative, neurogenic RPCs [37]. Consequently, impaired Yap1 or Hmga1a function
79 impedes MG reprogramming and neurogenesis in the regenerating retina [37]. In
80 contrast, the molecular and cellular identities of self-renewed MG and MG-derived
81 RPCs remain elusive. RPCs have fusiform nuclei that closely associate with GFAP-
82 positive glial fibers across the inner nuclear layer. They also express markers of
83 multipotency, like Pax6 and Sox2, as well as markers of neurogenesis, like Atoh7
84 [27,29,34,38,39]. Previous studies have investigated RPCs molecular identity mainly at the
85 population level [18,28,37,40–47]. However, a detailed characterization of the transcriptional
86 network underlying RPC production and RPC differentiation, as well as the lineage
87 relationships between MG, RPCs and differentiating progeny is currently missing.
88 Here, we profiled the transcriptome of MG and MG-derived RPCs in response to an
89 intense light lesion, and followed their differentiation trajectories towards regenerated
90 retinal neurons at the single cell level. In particular, we addressed the transcriptional
91 state of reactive MG prior to and after their asymmetric cell division. Moreover, we
92 addressed whether MG-derived RPCs are heterogeneous and to what extent they
93 express molecular markers that are observed during embryonic retinogenesis [48]. To
94 this aim, we employed a short-term lineage tracing strategy that allowed the isolation
95 of individual MG and MG-derived cells of the regenerating zebrafish retina, which were
96 subsequently subjected to droplet-based, 10x Genomics single cell RNA sequencing
97 (scRNAseq). We find that MG can be non-reactive in uninjured and lesioned
98 conditions, as well as reactive upon lesion. Reactive MG give rise to a hybrid cell
99 population, which replenishes the pool of MG as well as feeds into the pool of
100 neurogenic RPCs. Moreover, MG-derived RPCs are highly heterogeneous and display
101 a progressive restriction in their competence during subsequent differentiation. They

102 upregulate developmental markers of retinogenesis and produce regenerated neurons
103 partially according to the developmental birth order, with retinal ganglion cells born first
104 and bipolar cells born last.

105

106

107 **RESULTS**

108 **Isolation of individual MG, RPCs and regenerated progeny using fluorescent**
109 **reporters**

110 Previous work on the regenerating zebrafish retina described the early phases of MG
111 de-differentiation and RPC production [27,29,30,32,34,40,49]. However, knowledge on the
112 molecular identity and cell fate choices of RPCs is scarce and based on analyses at a
113 population level [18,28,37,40,42,43,45–47]. To study MG activation, RPC identity and their
114 relationship with MG in more detail, we profiled the transcriptome of MG and MG-
115 derived RPCs and followed their differentiation trajectories towards regenerated retinal
116 neurons at the single cell level. To do so, we devised a strategy to isolate individual
117 MG, RPCs and regenerated progeny, using retinae of uninjured and light-lesioned fish
118 carrying the two fluorescent reporters *pcna:EGFP* and *gfap:mCherry*. The former
119 drives the expression of EGFP under the regulatory elements of *proliferating cell*
120 *nuclear antigen* (*pcna*), a known marker of proliferating cells, and thereby labels
121 actively dividing cells, and, due to the persistence of EGFP, their short-term progeny.
122 The other reporter drives expression of mCherry under the regulatory elements of *glial*
123 *fibrillary acidic protein* (*gfap*), a known marker of zebrafish MG. Both transgenes
124 recapitulate the endogenous expression in the adult zebrafish retina faithfully
125 (supplemental figure 1). Immunohistochemistry against the proliferation marker PCNA

126 co-labeled *pcna:EGFP*-positive cells mainly in the ciliary marginal zone, one of the
127 stem cells niches in the adult zebrafish retina [16,39]. Occasionally, *pcna:EGFP*/PCNA-
128 double positive cells were observed in the central retina as well (supplemental figure
129 1A). The MG-specific antibody Zrf1 labeled virtually all *gfap:mCherry*-positive cells in
130 the central retina as well as in the ciliary marginal zone [16] (supplemental figure 1B).
131 We also addressed the expression of the two fluorescent reporter lines following light
132 lesion, at three different time points upon injury. First, 44 hours post light lesion (hpl),
133 when MG are about to undergo or have already completed their asymmetric cell
134 division giving rise to the first RPCs and self-renewed MG [27,49]. Second, 4 days post
135 light lesion (dpl), representing the peak of RPC proliferation [16,29] and third, 6 dpl, when
136 the first differentiating, regenerated progeny arise [16]. Immunohistochemistry against
137 EGFP and mCherry in double transgenic *Tg(pcna:EGFP);Tg(gfap:mCherry)* animals
138 corroborated the expected expression pattern of the transgenes in the central retina at
139 the chosen time points (supplemental figure 2). Uninjured, central retinae displayed no
140 EGFP, but strong mCherry signal consistent with non-proliferating MG (white
141 arrowheads). In contrast, numerous EGFP/mCherry double-positive cells were present
142 at 44 hpl, indicating potential cell-cycle re-entry of MG (yellow arrowheads). At 4 dpl,
143 overall mCherry expression was reduced, consistent with the previously described
144 downregulation of the *gfap* promoter by MG-derived RPCs. In contrast, EGFP was
145 strongly found throughout all retinal layers, matching the reported peak in proliferation
146 of MG-derived RPCs (red arrowheads) [16,17,25,28,29]. Finally, in comparison to 4 dpl, an
147 increase in mCherry accompanies a decline in EGFP signal at 6 dpl (yellow
148 arrowhead). In order to obtain single cells of MG, RPCs and regenerated progeny, we
149 utilized the persistence of EGFP and mCherry fluorescence, providing a short-term
150 label. Initially, only MG express mCherry in uninjured, central retinae, but activate
151 EGFP in preparation of the asymmetric cell division upon light lesion at 44 hpl (Figure

152 1A). Firstborn RPCs inherit high levels of persisting fluorescent mCherry protein from
153 dividing MG and slowly degrade/dilute the protein during subsequent rounds of cell
154 division. Hence, MG-derived, but further dividing, RPCs are EGFP-positive, but low
155 mCherry-positive at 4 dpl. At 6 dpl, RPCs have further diluted the mCherry reporter,
156 thus displaying only a faint mCherry signal, but remain EGFP-positive. Similarly, RPC-
157 derived, regenerated progeny is characterized by even lower levels of intrinsic
158 mCherry fluorescence, and low EGFP signal during subsequent cell differentiation at
159 6 dpl. Following this rationale, we dissected retinae of uninjured and light-lesioned
160 samples, dissociated them into single cell suspensions that were subjected to flow
161 cytometry followed by droplet-based, 10x Genomics scRNAseq (Figure 1B). Flow
162 cytometry plots confirmed the rationale of the above-mentioned strategy (Figure 1C).
163 In all samples, we detected non-fluorescent and EGFP-positive only cells, consistent
164 with non-proliferating and proliferating cells in the adult zebrafish retina. We also
165 detected cell populations expressing only mCherry at all sampled time points, most
166 likely representing non-reactive MG. In addition to cells expressing either EGFP or
167 mCherry, we find EGFP/mCherry-double positive cells in all samples consistent with
168 proliferating MG originating from the ciliary marginal zone and the central retina (see
169 supplemental figure 1 and 2). The EGFP/mCherry-double positive population
170 increased at 44 hpl, presumably due to an increase in the cell number of reactive,
171 proliferating MG. At 4 dpl, the expanded EGFP/mCherry-double positive cell population
172 was still present, but displayed a lower mCherry, yet an increased EGFP signal, in line
173 with MG-derived RPCs, peaking in proliferation [16,29]. At 6 dpl, a further decreased
174 mCherry intensity was observed for the EGFP/mCherry-double positive cell population.
175 In order to profile the transcriptome of individual MG, RPCs and progeny of the
176 uninjured and light lesioned retinae, we dissected retinae of the before-mentioned time
177 points (uninjured, 44 hpl, 4 dpl, 6 dpl) and eventually sorted 15.000 cells per time point.

178 We applied a sorting gate that included both mCherry-positive only and
179 EGFP/mCherry-double positive cells at the sampled time points (Figure 1C). Non-
180 fluorescent as well as EGFP- only positive cells were not included. Taken together, we
181 devised a short-term lineage tracing strategy that allows the isolation of individual MG
182 and MG-derived cells of the regenerating zebrafish retina, which can be subjected to
183 droplet-based,10x Genomics.

184

185 **scRNAseq identifies 15 distinct cell populations in the light-lesioned retina**

186 Sorted cells underwent 10x Genomics scRNAseq and 13.139 cells passed the
187 sequencing quality control. We detected a median of 1.407 genes and 4.061 mean
188 read counts per cell. Initially, we identified three clusters for the full dataset
189 (supplemental figure 3A): a retinal core dataset and two additional clusters identified
190 as microglia and low-quality cells expressing many ribosomal transcripts
191 (supplemental figure 3A, B). Both populations were excluded from the subsequent
192 analysis. Re-clustering of the core dataset, which eventually included 11.690 cells,
193 revealed 15 potential, different cell populations (Figure 2A). From left to right on the
194 UMAP, which visualizes the cell lineage trajectory, we observed the progressive
195 emergence of MG, RPC and progeny clusters. We assigned the cellular identity by
196 inspecting the top 100, upregulated marker genes per cluster (supplemental table 1).
197 In detail, we identified four MG clusters (clusters 1 to 4) that locate to the left and middle
198 portion of the map, followed by five RPC clusters (clusters 5 to 9) locating to the right
199 side of the map. Regenerated progeny branch from the RPCs and include retinal
200 ganglion (cluster 10), amacrine (cluster 13) and bipolar cells (cluster 15) at the bottom-
201 right, as well as red and blue cones (clusters 11 and 12) at the top-right of the map.

202 Additionally, there is a second cluster of amacrine cells (cluster 14) that separates from
203 the first amacrine cell cluster.

204 To investigate how the composition of cells changed during regeneration, we
205 computed embedding densities for each time point (Figure 2B). Similar to the
206 progression of cellular identities, cells progressed over time from left to right, from the
207 uninjured, to the 44 hpl, the 4 dpl, as well as the 6 dpl enriched samples. As expected,
208 cells belonging to non-reactive MG were found at all sampled time points. In particular,
209 the vast majority of cells of the uninjured sample belonged to cluster 1 as well as cluster
210 2. However, we also observed a small proportion of cells (Figure 2B) aligning in a
211 trajectory from non-reactive MG (left side of the map) through reactive MG (middle
212 part) to RPCs and differentiating progeny (right side) in the uninjured sample. At 44
213 hpl, cells mapping to non-reactive MG were still abundantly present, although mostly
214 shifted right towards a cluster representing reactive MG (cluster 3). Cells belonging to
215 this cluster of reactive MG were also highly enriched in this sample. In contrast, cells
216 mapping to the second cluster of reactive MG (cluster 4) as well as to RPCs (clusters
217 5-9) were overrepresented at 4 dpl, in line with the reported peak in proliferation at this
218 time point [16,29]. Cells mapping to RPCs were still frequently present at 6 dpl. Moreover,
219 cells belonging to regenerated progeny (clusters 10-15), which first appear at 4 dpl,
220 became predominantly enriched at 6 dpl. In addition to the overall progression from left
221 to right, we noted that cells mapping to reactive MG of the second cluster (cluster 4)
222 and the abutting portion of non-reactive MG (cluster 1) were also enriched at this time
223 point, indicating a reversed direction.

224 Analysis of the cell cycle state further supported our cluster annotation. Specifically,
225 known cell cycle marker genes were used to calculate the predicted cell cycle state [50–
226 52], and the cell cycle phase (G1, S, G2/M) was projected onto the UMAP of the single

227 cell transcriptome (Figure 2C). Differentiating or differentiated cells were considered
228 as cells in G1 [53]. Consistently, we observed that most cells of the left side and lower
229 middle part as well as cells branching from the right side of the map were in G1, which
230 comprised most non-reactive MG (clusters 1 and 2), one cluster of reactive MG (cluster
231 4), one RPC population (cluster 7) and the regenerated progeny (clusters 10-15). Cells
232 in S phase were also present on the left side of the map, which represent non-reactive
233 MG (clusters 1 and 2), but were in particular enriched in two domains of the middle
234 part corresponding to reactive MG (cluster 3) and RPCs (clusters 5 and 7). In addition,
235 two domains on the right side of the map showed an accumulation of cells in S phase,
236 which include photoreceptor and horizontal cell precursors (clusters 8 and 9). The
237 pattern of cells in G2/M phase complemented the pattern of cells in G1 and S phase.
238 Cell proliferation pattern was further confirmed by *pcna* expression (Figure 2D). When
239 plotting *pcna* expression onto the main UMAP of the single cell transcriptome, we
240 observed high counts in one population of reactive MG (cluster 3) and in RPCs
241 (clusters 5, 6, 8 and 9). In summary, scRNAseq analysis enabled the establishment of
242 a transcriptome map, which reveals the progressive emergence of non-reactive MG,
243 reactive MG and MG-derived progenitors and regenerated progeny.

244

245 **scRNAseq identifies two populations of non-reactive and two of reactive MG in**
246 **the light-lesioned retina**

247 MG in the homeostatic zebrafish retina are characterized by the expression of GFAP,
248 as well as other canonical glial markers, like *apoeb*, *glula*, *cahz*, *rlbp1a* [28,39,54–56]. In our
249 scRNAseq dataset, we found clusters 1 and 2 expressing *apoeb*, *glula*, *cahz*, *rlbp1a*
250 as marker genes (supplemental figure 4 and supplemental table 1). When plotting
251 *apoeb* expression onto the UMAP, we observed high counts in clusters 1 and 2, as

252 well as in clusters 3 and 4 (Figure 3A). The glial marker *gfap*, found among the top 100
253 upregulated marker genes for cluster 4 (supplemental table 1), showed a similar
254 pattern, with high counts in clusters 1 to 4, but displayed high counts in cluster 5 as
255 well (Figure 3A). Given the expression pattern of *apoeb* and *gfap*, we identified clusters
256 1 to 4 as MG populations. Further analysis indicated clusters 1 and 2 as non-reactive
257 MG and clusters 3 and 4 as reactive MG (Figure 3B, C). Non-reactive MG, which were
258 mostly in G1 and did not express any injury-specific markers (supplemental figure 4)
259 showed counts for *mstnb* (Figure 3B). In addition, members of the retinoic acid
260 signalling pathway, like *rdh10a*, *aldh1a3*, *dhrs3a* [57–59] were enriched in these clusters
261 (supplemental figure 5A, supplemental table 2).

262 We next looked into differentially expressed genes (DEG) between the non-reactive
263 MG clusters 1 and 2. For instance, the UMAP plot of *inhbaa*, an evolutionarily
264 conserved vertebrate glia marker [37] showed strong expression only in clusters 1, 3 and
265 4, but not in cluster 2 (Figure 3B, supplemental figure 5A, and supplemental table 2).
266 Reactive MG on the other hand downregulated some glial markers, like *glula* and
267 *rlbp1a*, and upregulated inflammatory cytokines, like *crlf1a*, matrix metalloproteases,
268 like *mmp9*, and growth factors like *hbegfa* in the regenerating retina (supplemental
269 figure 4, 5B, and supplemental table 1). Consistent with that, plotting of *crlf1a*
270 expression onto the UMAP showed high read counts in clusters 3 and 4, as well as in
271 cluster 5 (Figure 3C). Again, DEG analysis showed that reactive MG can be subdivided
272 further, because only cluster 3, but not cluster 4 expressed Hairy-related downstream
273 targets of active Notch signalling including *her15.1-1*, *her9* and *her4.1* (supplemental
274 figure 4, 5B, and supplemental table 3). Indeed, the UMAP plot of *her4.1* showed
275 strong expression in cluster 3 as well as in cluster 5 (Figure 3C). To validate the
276 expression of *her4.1* in the regenerating retina we used *in situ* hybridization. In
277 agreement with our scRNAseq dataset, *her4.1* signal was not present in the uninjured

278 retina, but appeared at 44 hpl in the inner nuclear layer of the central retina (Figure
279 3D). At 4 and 6 dpl, *her4.1* transcripts remained in the inner nuclear layer and appeared
280 in cells of the outer nuclear layer too (Figure 3D). We further analysed the expression
281 of *crlf1a*, a marker of reactive MG, with fluorescent *in situ* hybridization combined with
282 immunohistochemistry against GFAP (located mainly to MG fibers) and the
283 proliferation marker PCNA (Figure 4). Consistent with our scRNAseq dataset, *crlf1a*
284 was not detectable in the uninjured, central retina, but was upregulated in Zrf1/PCNA-
285 double positive cells at 44 hpl (Figure 4A, B). At 4 dpl, *crlf1a* signal was still present in
286 Zrf1/PCNA-double positive cells and returned back to undetectable levels at 6 dpl
287 (Figure 4A, B). Taken together, we observed cellular heterogeneity in MG during
288 regeneration, and identified two non-reactive and two reactive MG populations that
289 express distinct marker genes.

290

291 **scRNAseq identifies a transient cell population with hybrid characteristics of**
292 **reactive MG and early RPCs in the light-lesioned retina**

293 As mentioned above, several MG-related genes, like *gfap* or *crlf1a*, were also
294 expressed in cluster 5, which locates next to the reactive MG (clusters 3 and 4), is
295 highly proliferative and only becomes eminent at 4 dpl. Further analysis of this cluster
296 showed expression of several members of the High Mobility Group (Hmg) protein
297 family among the top 100 upregulated marker genes (supplemental table 1).
298 Consistent with that, the UMAP expression profile of *hmgb2b* showed presence of high
299 counts already in cluster 3 (reactive MG), as well as in other, further downstream RPC
300 clusters and regenerating progeny (Figure 5A). This indicated a transition from MG to
301 RPC fate in the course of regeneration and that cells of cluster 5 might have hybrid
302 characteristics of reactive MG and downstream RPCs. Hence, we conducted a DEG

303 analysis of cluster 5 in comparison to reactive MG (clusters 3 and 4), as well as to the
304 neighbouring, downstream RPCs (cluster 6). When compared to reactive MG, cells of
305 cluster 5 showed expression of several genes, including *stmn1a*, *nr2e1* and *sox9b*
306 (supplemental figure 5C, supplemental table 4 and 5). Consistently, UMAP expression
307 profile of *stmn1a* showed counts prevalently in cluster 5 and neighbouring,
308 downstream RPCs on the right side of the map, but not in the reactive or non-reactive
309 MG on the left side (Figure 5A). The UMAP profiles of *sox9b* and *nr2e1* showed strong
310 expression almost exclusively restricted to cluster 5. DEG analysis between cluster 5
311 and the neighbouring downstream cluster 6 revealed also expression of *nr2e1* and
312 *sox9b*, but additionally transcripts like *id1* (supplemental figure 5D and supplemental
313 table 6). Consistently, high *id1* counts were found in cluster 5 and in other reactive or
314 non-reactive MG clusters, but not in downstream RPCs on the right side of the map
315 (Figure 5A). In order to validate the RNAseq data, we analysed the expression of
316 *hmgb2b* and *id1* transcripts in the regenerating retina using *in situ* hybridization and
317 fluorescent *in situ* hybridization combined with immunohistochemistry, respectively.
318 Consistent with our scRNAseq data, *hmgb2b* signal was not detectable in the
319 uninjured, central retina, but was initiated in individual cells residing in the inner nuclear
320 layer at 44 hpl (Figure 5B). Subsequently, *hmgb2b* transcripts could be detected in
321 clusters of cells in the inner and outer nuclear layers at 4 and 6 dpl (Figure 5B). The
322 expression of *id1* in the regenerating tissue matched the scRNAseq data. Expression
323 of *id1* was already detectable in Zrf1-positive but PCNA-negative cells in the inner
324 nuclear layer of the uninjured, central retina (Figure 6A, B). At 44 hpl, *id1* was strongly
325 upregulated and co-localized with Zrf1/PCNA-double positive cells in the inner nuclear
326 layer. At 4 and 6 dpl, *id1* expression was still associated with Zrf1/PCNA-double
327 positive cells and, occasionally, with PCNA-only positive cells (Figure 6A, B). In
328 summary, marker analysis reveals that cells in cluster 5 display a transcriptional

329 signature of reactive MG, as well as RPCs, which is why we assigned it a hybrid
330 identity.

331

332 **scRNAseq identifies two neurogenic progenitor populations in the light-lesioned**
333 **retina**

334 The before-mentioned DEG-analysis between cluster 5 (hybrid cells) and cluster 6
335 (neighbouring, downstream RPCs) also revealed that the latter upregulated *insm1a*
336 (supplemental figure 5D and supplemental table 6), which has been described to
337 promote cell cycle exit of RPCs in the injured fish retina at 4 dpl [47]. In addition, our
338 DEG analysis showed upregulation of *atoh7* and *onecut2* in cluster 6 (supplemental
339 figure 5D and supplemental table 6). We found that the highly redundant gene *onecut1*
340 was also expressed in cluster 6, albeit this was not found in the DEG analysis. As
341 expected, the UMAP expression profile of *insm1a* confirmed high read counts in cluster
342 6 but also in clusters 7, 8 and 10 (Figure 7A). The UMAP expression profile of *atoh7*
343 also confirmed expression in cluster 6, as well as in clusters 7 and 10 (Figure 7A).
344 Moreover, the UMAP expression profile of *onecut1* and *onecut2* confirmed that both
345 genes were expressed in clusters 6 and 7 and in addition in cluster 9 (Figure 7A).
346 Cluster 7 expressed additional neurogenic marker genes like *tubb5* and *sox11b* [60–62]
347 (supplemental figure 5D and supplemental table 1). Finally, the cell cycle status and
348 the UMAP expression of *mki67,* a mitotic marker, showed read counts in cluster 6, but
349 not in cluster 7 (Figure 7A). Hence, we concluded that cluster 6 and cluster 7
350 represented neurogenic progenitors, and were named progenitors 2 and progenitors
351 3, respectively. To validate *atoh7*, *onecut1* and *onecut2* expression in the regenerating
352 retina, we employed again *in situ* hybridization. In agreement with our scRNAseq data,
353 *atoh7* signal was absent in the uninjured and 44 hpl retina, but became detectable in

354 the inner and outer nuclear layers at 4 and 6 dpl (Figure 7B). Similarly, *onecut1* and
355 *onecut2* were prominently expressed in the inner and outer nuclear layer at 4 and 6
356 dpl, in addition to their homeostatic expression in the presumptive horizontal cell layer
357 in the uninjured and 44 hpl retina (Figure 7B, black arrowheads). In summary,
358 scRNAseq showed heterogeneity of neurogenic progenitors, which upregulate known
359 markers of retinogenesis in the regenerating retina.

360

361 **scRNAseq identifies fate-restricted progenitors in the light-lesioned retina**

362 Gene expression analysis of cluster 8, which locates next to the neurogenic
363 progenitors (cluster 6 and 7), showed significant upregulation of several well-known
364 photoreceptor precursor markers, including *crx*, and *thrb* (supplemental table 1).
365 Consistently, UMAP plots for *crx* and *thrb* revealed high counts in cluster 8 (Figure 8A).
366 Moreover, the former was also highly expressed in clusters 11 and 12, whereas the
367 latter was restricted to the additional cluster 1. Subsequent further gene expression
368 analysis identified clusters 11 and 12 as differentiating cone photoreceptors arising
369 from cluster 8. Precisely, clusters 11 and 12 represent differentiating photoreceptors
370 giving rise to blue and red cones as shown by the UMAP plots of *opn1sw2* and
371 *opn1lw2*, respectively (Figure 8B). Cluster 9, which abuts the neurogenic progenitor 3
372 (cluster 7), expressed known developmental markers of horizontal cell precursors like
373 *prox1a* and *rem1* (supplemental table 1). Consistently, the UMAP plot for *rem1* showed
374 high expression almost restricted to this cluster specifically. Gene expression analysis
375 also revealed *ptf1a* expression in cluster 9, which has been shown to be required for
376 lineage specification of horizontal and amacrine cells in the developing retina [63,64]. In
377 line with these findings, the UMAP expression profile of *ptf1a* confirms high counts in
378 the left part of cluster 9, but is even more pronounced in the upstream part of cluster 7

379 feeding into cluster 9 (Figure 8C). Gene expression analysis of the remaining clusters
380 10, 13, 14 and 15 identified them as differentiating progeny giving rise to retinal
381 ganglion cells (cluster 10), amacrine cells (clusters 13 and 14), as well as bipolar cells
382 (cluster 15), respectively (supplemental table 1). In this context, UMAP plots of *gap43*
383 and the more mature retinal ganglion cell marker *isl2b* showed a strong upregulation
384 in cluster 10 (Figure 8D). UMAP plots of *stx1b* and *pvalb6*, markers of differentiating
385 and mature amacrine cells, revealed strong expression in clusters 13 and 14, whereas
386 UMAP plots of *vsx1* and *samsn1a*, known and novel markers of bipolar cells,
387 respectively, showed high counts in cluster 15 (Figure 8E, F).

388 With this respect, it was recently shown that the regenerating adult zebrafish retina
389 recapitulates developmental fate specification programs [43]. Hence, we plotted the
390 fraction of cells that differentiate into a specific cell fate during the time course of
391 regeneration (supplemental figure 6). We found that the earliest committed progeny
392 emerged at 4 dpl giving rise to retinal ganglion cells or to photoreceptors, in particular
393 red cones. At 6 dpl, the number of retinal ganglion cells and red cones continued to
394 increase. In addition, we detected a significant number of blue cones and amacrine
395 cells, as well as a small number of bipolar cells at this time point. We did not detect
396 any differentiating progeny giving rise to horizontal cells or rods at this stage. To
397 address this issue, we further investigated the expression of more mature neuronal
398 markers in our dataset (supplemental figure 7). Expression of *rho* and *gnat1*, two
399 markers of rod photoreceptors, was very low and sparse, and did not define any
400 specific rod cluster (supplemental figure 7A). Expression of *gad1b*, which encodes for
401 glutamate decarboxylase synthetizing the neurotransmitter GABA, was mostly
402 restricted to amacrine cells (clusters 13 and 14) (supplemental figure 7B). To address
403 the expression of more mature markers of amacrine and horizontal cells, we
404 investigated *chata* (*choline O-acetyltransferase a*, an amacrine cell-specific marker),

405 as well as *calb2a* and *calb2b* (*calbindin 2a* and *calbindin 2b*, markers of amacrine and
406 horizontal cells) (supplemental figure 7B, C). As expected, high counts of *chata* were
407 specifically found in amacrine cells (clusters 13 and 14). In particular, *chata* expression
408 was detected only in cells located at the tip of cluster 13 and in all cells of cluster 14.
409 *calb2a* was expressed in some reactive MG (cluster 3) and quite strongly in some
410 amacrine cells (cluster 13). Importantly, we did not detect any *calb2a* and *calb2b* in
411 horizontal cell precursors (cluster 9).

412 We also checked the expression of transcripts for variants of protein kinase C using
413 *prkcab* and *prkcbb* (*protein kinase alpha b*, *protein kinase beta b*) to identify mature
414 bipolar cells (supplemental figure 7D). Counts for *prkcab* were sparsely found in some
415 non-reactive and reactive MG (clusters 1-4). *prkcbb*-positive cells were found more
416 frequently in some non-reactive and reactive MG (clusters 1-4), progenitor 1 (cluster
417 5), as well as in amacrine cells (clusters 13, 14). Importantly, we did not detect *prkcab*
418 or *prkcbb* in our bipolar cells. When plotting the expression of general synaptic markers
419 like *snap25a* and *snap25b*, we observed mainly transcripts in the differentiating
420 progeny (supplemental figure 7E). Specifically, high counts of *snap25a* were found in
421 retinal ganglion and amacrine cells (clusters 10, 13 and 14). High counts of *snap25b*
422 were observed in the same clusters as well as in red and blue cones (clusters 11 and
423 12) and the right part of the horizontal cell precursors (cluster 9). Taken together, our
424 scRNAseq data reveal the presence of fate-restricted progenitors and the sequential
425 appearance of differentiating progeny in the light-lesioned, adult zebrafish retina.
426 Moreover, the analysis of more mature markers shows that the differentiation of retinal
427 ganglion cells and red cones is preceding the appearance of blue cones, amacrine and
428 bipolar cells.

429

430 **DISCUSSION**

431 In this study, we employed a short-term lineage tracing strategy, which allowed the
432 selective enrichment of MG and their respective progeny for up to six days post light
433 lesion. Subsequent scRNAseq resolved the transcriptome of individual MG, RPCs as
434 well as regenerated progeny, and allowed to reconstruct their lineage relationship in
435 the homeostatic and regenerating zebrafish retina (Figure 1). A previous study
436 combined bulk RNA sequencing of sorted MG with scRNAseq of whole retinae from
437 zebrafish upon NMDA as well as light lesions [37]. This work focussed specifically on the
438 early reprogramming of MG and progenitor production, covering up to 36 hours post
439 light lesion. The authors report that MG go through an activated, non-proliferative state
440 characterized by upregulation of gliosis markers. However, neither did they find any
441 evidence of MG heterogeneity in uninjured conditions nor did they provide any
442 thorough characterization of MG-derived RPCs [37]. Additional RNA sequencing studies
443 of the regenerating zebrafish retina have used microarray as well as RT-PCR and qRT-
444 PCR to evaluate transcriptional changes at a population level, without providing any
445 MG/RPC single cell resolution [40–42,44–46,65]. Previous immunohistochemistry and *in situ*
446 hybridization experiments provided a broad description of MG-derived RPCs. Indeed,
447 progenitors are reported as fusiform cells that proliferate and express markers of
448 multipotency like Pax6 and Sox2, as well as some neurogenic markers like Atoh7,
449 Ptf1a, Vsx1 and others [16,17,29,38,43,47]. In contrast to these previous results, our study is
450 the first providing a comprehensive overview of MG, MG-derived cells and their lineage
451 relationship up to 6 days post lesion in the zebrafish retina. Due to our selective
452 enrichment of MG and their respective progeny, we gain an adequate single cell
453 resolution to observe substantial heterogeneity in the molecular identity of MG in
454 homeostatic as well as regenerating conditions. We also provide an in depth
455 description of MG as well as RPC molecular identity, cell fate decisions and production

456 of regenerated progeny that cover all key aspects during zebrafish retina regeneration.
457 Our strategy allowed us to define two main trajectories in the regenerating zebrafish
458 retina (Figure 9). The first trajectory (solid and dashed red lines) comprises clusters 1
459 to 5 and constitutes a closed cycle that both maintains the MG pool and generates the
460 first-born neurogenic RPCs. The second trajectory (solid black lines) involves clusters
461 6 to 15 and gives rise to all retinal neurons via the progressive restriction in cell fate
462 competence of neurogenic RPCs. We discuss the two trajectories separately.

463

464 **Müller glia self-renew and give rise to early, multipotent progenitors**

465 The glial trajectory starts with non-reactive MG (clusters 1 and 2), which express
466 canonical glial markers like *gfap*, *apoeb* and additional genes like *glula*, *rlbp1a* and
467 *cahz* that ensure the housekeeping function of MG during homeostasis (Figure 3A,
468 supplemental figure 4, supplemental table 1). Most cells in the non-reactive MG
469 clusters are quiescent based on the analysis of the cell cycle, and are frequently found
470 in the uninjured, but also in the lesioned retina at all sampled time points (Figure 2).
471 However, some non-reactive MG are in S or G2/M phases of the cell cycle, and
472 express *pcna*, albeit at a lower level as compared to the expression in injury-induced,
473 proliferating cell clusters (Figure 2C, D). This is consistent with the proposed model
474 that zebrafish MG proliferate occasionally also in the uninjured, central retina and
475 generate rod progenitors that feed the rod precursor pool at the base of the outer
476 nuclear layer [10,16]. Accordingly, we detect PCNA-positive cells in the uninjured, central
477 retina (supplemental figure 1) as well as a small fraction of cells that align in a trajectory
478 from non-reactive MG on the left through reactive MG in the middle, to photoreceptor
479 precursors on the right side of the UMAP in the uninjured retina (Figure 2B). However,
480 some cells end up in the amacrine as well as retinal ganglion cell clusters. This

481 suggests that MG might have the potential to generate not only rods, but also all other
482 retinal neurons in the homeostatic adult retina. Indeed, MG in the uninjured retina
483 express, albeit at a low level, multipotency markers like *pax6*, and share many marker
484 genes with RPCs [16,39,66]. Still, MG and injury-induced RPCs are considered distinct cell
485 populations. Upon injury, MG divide only once between 31 and 48 hpl, whereas MG-
486 derived RPCs continue to divide, reaching a peak of proliferation at 4-5 dpl (discussed
487 in [25,28,29,43]). We isolated cells at 44 hpl, a time point when MG are about to undergo,
488 or already underwent, their asymmetric cell division [16,25,27,49] and identify cells in cluster
489 3 as early reactive MG. Consistent with that, we find that cells in cluster 3 do not only
490 express *gfap* and *apoeb*, but also *pcna* (Figure 2D, 3A). Moreover, the predicted cell
491 cycle status supports this notion. Whereas cells in the left part of cluster 3 are mostly
492 in G1, cells in G2/M phase are found in the right part, with cells in S phase overlapping
493 with both domains (Figure 2C). Cells in cluster 3 also upregulate inflammation-related
494 markers like *crlf1a*, as well as *mmp9* and *hbegfa* (Figure 3C, 4, supplemental figure 5B
495 and supplemental table 1). The upregulation of inflammatory genes makes MG similar
496 to immune cells [35,36,67]. In this context, our population of early reactive MG (cluster 3),
497 identified mostly at 44 hpl, resembles the reactive MG pool found in the regenerating
498 zebrafish retina at 36 hpl [37]. However, our MG cluster is proliferative, whereas the one
499 discussed by the mentioned study is not. The presence of a distinct pool of non-
500 proliferative, reactive MG as early as 36 hpl in the earlier study might be explained by
501 the different time points of sample collection, and/or by the lower number of cells
502 sequenced in our experiment (11.690) in comparison to the previous one (45.153) [37].
503 In summary, MG in the homeostatic zebrafish retina behave like multipotent RPCs.
504 Upon injury, reactive MG express genes associated with inflammation, like *crlf1a*, and
505 undergo asymmetric cell division. Daughter cells derived from this cell division most
506 likely map to cluster 5, which is discussed below.

507

508 **A crossroad in the glial trajectory: hybrid cells with MG and RPC characteristics**

509 The close similarity between zebrafish MG and MG-derived RPCs at the level of
510 expressed markers as well as cellular and subcellular morphology has been described
511 extensively in the literature [24,25,29]. Thus, we suggest that cells in cluster 5, which
512 displays a transcriptional hybrid identity between MG and RPCs, are the product of the
513 asymmetric cell division from the early reactive MG (cluster 3). Cells in cluster 5 are
514 still *gfap* positive, and share marker expression with early reactive MG, like *her4.1* and
515 *crlf1a* (Figure 3A, C). However, cluster 5 is highly proliferative and becomes only
516 prominent at 4 dpl, a time point when predominantly RPCs are proliferating [16,25,27,29].
517 Consistently, *pcna* is highly expressed in cluster 5 and the predicted cell cycle status
518 indicates that most cells are in S or G2/M phase (Figure 2C, D). Moreover, previous
519 studies have found *her4.1* and *crlf1a* in MG-derived RPCs in the light- as well as stab-
520 lesioned retina, where they control RPC proliferation at 4 dpl [35,36,68]. We found that
521 *her4.1* at 4 and 6 dpl locates to the inner nuclear layer as well as to the outer nuclear
522 layer, where presumptive RPCs reside at this time point (Figure 3D) [68,69]. In addition,
523 cells in cluster 5 upregulate *sox9b* and *nr2e1*, which have been found in early,
524 multipotent RPCs of the developing fish, avian and mammalian retinae, as well as in
525 late retinogenesis, where they regulate MG genesis [70–74]. Hence, we propose that cells
526 in cluster 5 represent a crossroad of the glial and neurogenic trajectory, containing self-
527 renewed MG as well as first-born, MG-derived RPCs as a direct result of the earlier
528 (44 hpl) asymmetric MG cell division. We further propose that self-renewed MG close
529 the cycle via late reactive MG (cluster 4) and return into non-reactive MG (clusters 1
530 and 2, red, dashed line in Figure 9). In contrast, MG-derived RPCs embark into the
531 neurogenic pathway (cluster 6, solid, black line). In an alternative model, cells in cluster

532 5 might represent only MG cells that have upregulated early RPC markers like *sox9b*
533 and *nr2e1* and are dividing a second time at 4 dpl to generate renewed MG (cluster 4)
534 and neurogenic RPCs (cluster 6). However, MG have been described to divide only
535 once between 24 and 42 hpl and additional and/or asynchronous MG divisions later
536 than 2 dpl have not been investigated [25,27,49]. BrdU/EdU lineage tracing experiments
537 will be required to address this issue, with the caveat that MG and RPCs are hardly
538 distinguishable from each other in the 4 dpl retina, especially when using the Zrf1
539 antibody to label MG [29,39]. Live imaging of the regenerating retina would be the best
540 tool to follow MG and MG-derived progenitors *in vivo*, but the technique is not optimized
541 yet for long recordings from the intact tissue in the living animal [49]. Either way, our
542 proposed model of self-renewing MG is further supported by the change of cell density
543 over time (Figure 2B). Following the cells across the four time points on the UMAP, we
544 observe that initially most cells of the uninjured sample map to non-reactive MG
545 (clusters 1 and 2) located at the far left. At 44 hpl, the cell density shifts towards the
546 upper right portion of cluster 1 and towards the early reactive MG (cluster 3) in the
547 upper, middle of the map. At 4 dpl, sampled cells mostly map to RPCs (clusters 5-9)
548 on the right, as well as to late reactive MG (cluster 4) in the lower, middle part.
549 Additionally, cells mapping to the lower right part of non-reactive MG (clusters 1 and
550 2) are enriched in this sample, indicating a reverse direction from right to left. This
551 population is significantly further increased at 6 dpl, when the number of RPCs is less
552 prominent and the differentiating neural types at the top and bottom right are
553 predominantly present in the sample. According to this model, sample collection at
554 even later time points, e.g. 10 or 14 dpl, might show that the initial status has been
555 restored and that non-reactive MG are mostly enriched. However, it is unlikely that this
556 experiment could be performed with our short-term labelling strategy.

557

558 **The neurogenic trajectory produces regenerated progeny that partially follow**
559 **the developmental order of neurogenesis**

560 Neurogenic RPCs map to the right of cluster 5, and include proliferating, neurogenic
561 RPCs (cluster 6) and the downstream, non-proliferating, neurogenic RPCs (cluster 7).
562 Cells in these clusters express *insm1a*, *atoh7* and additional neurogenic genes that
563 are required for the generation of several neuronal lineages (Figure 7, supplemental
564 figure 5D and supplemental table 1 and 6). Indeed, *atoh7* expression has been
565 described to be initiated in RPCs on their way to the last cell division giving rise to a
566 retinal ganglion cell and another cell that can be either an amacrine cell, or a precursor
567 of a horizontal or of a cone cell in the developing zebrafish retina [2,75,76]. Cluster 6 and
568 7 appear also highly similar to the transient, neurogenic RPC state that has been
569 described recently in the developing mouse retina [53]. We propose that cluster 6 and 7
570 are the roots of the neurogenic trajectory from which fate-restricted RPCs and
571 regenerated progeny arise at 4 and 6 dpl (solid, black line in Figure 9). Cells in cluster
572 6 are *mki67*-positive, but additionally express *insm1a*, which promotes RPC cell cycle
573 exit at 4 dpl in the injured retina [47]. Cells in cluster 6 might undergo their last cell
574 division, as suggested by the concomitant expression of *atoh7*. Consistently, in our
575 scRNAseq high counts of *atoh7* are found in cells of cluster 6, to cluster 7 and
576 eventually cluster 10. Cluster 10 represents differentiating retinal ganglion cells that
577 are the first regenerated progeny, evident as early as 4 dpl (Figure 7, 9 and
578 supplemental figure 6).

579 While amacrine cells arise directly from the core of neurogenic RPCs, fate restricted
580 precursors for regenerated cones and for horizontal cells are identified (Figure 8 and
581 9), as it occurs during development [12,77]. Consistently with the events during
582 development, red cones (cluster 11) branch from *thrb*-positive cells of the

583 photoreceptor RPC cluster (cluster 8). Interestingly, *thrb* transcripts are found in
584 neurogenic RPCs of cluster 7 as well as at the beginning of cluster 9, which contains
585 horizontal cell precursors becoming evident at 4 dpl (Figure 8B). This is in agreement
586 with observations in the developing zebrafish retina, where horizontal and cone cells
587 share a common Thrb-positive progenitor [78]. Mature markers of horizontal cells, like
588 calbindins, are not found in cluster 9 (Figure 8B, supplemental figure 6C and
589 supplemental table 1), in contrast to cone photoreceptor mature markers, like opsins,
590 at 4 and 6 dpl. While it might be that mature horizontal cells arise later than 6 dpl, their
591 absence from our dataset could also be due to our experimental set-up. As explained
592 before, we isolated mCherry-only positive and EGFP/mCherry-double positive cells to
593 obtain MG and MG-derived cells. Whereas mCherry, driven by a *gfap* promoter
594 fragment, is actively transcribed in MG, the label of MG-derived cells is completely
595 dependent on the half-life of the fluorophore. Protein turnover and further cell divisions
596 would result in a constant depletion of mCherry in MG-derived cells over time. In this
597 context, we find a strong expression of *pcna* in cluster 9, indicating that additional cell
598 divisions might have diluted the mCherry label to undetectable levels (Figure 2D).
599 Inclusion of EGFP-positive only cells in our sample collection may reveal the pool of
600 mature horizontal cells, which inherit the fluorophore from their *pcna:EGFP*-positive
601 precursors. Accordingly, we find the presence of horizontal cell precursor markers in
602 our dataset. For instance, cells in cluster 9 express *onecut1* and *onecut2*, which
603 encode transcription factors and are upregulated in horizontal cell RPCs in the
604 developing mouse retina, and which regulate horizontal cell maintenance in adult
605 animals [79–81]. Counts for *onecut1* and *onecut2* are found also in earlier neurogenic
606 RPCs of clusters 6 and 7, where they most likely contribute to the transient state of
607 RPCs together with additional neurogenic markers, like *atoh7* [53]. This is again
608 consistent with observations in the developing mouse retina, where Onecut1 and

609 Onecut2 regulate the development of retinal ganglion cells, as well as the development
610 of cones, horizontal cells, and of a subset of amacrine cells, while inhibiting rod
611 specification genes [79,81].

612 In addition to mature horizontal cells, we were also unable to detect any rod-specific
613 cluster expressing mature rod markers like *rho* and *gnat1* (supplemental figure 7A).
614 We assume that mature rods might arise as a third branch from the photoreceptor RPC
615 cluster (Figure 9), which indeed expresses rod specification markers like *nr2e3*
616 (supplemental table 1). We speculate that rods either become evident only later than
617 6 dpl, or that they do not survive the isolation procedure, since rods possess a complex
618 morphology with long outer segments. A third possibility might be that rod
619 photoreceptors are replenished by their dedicated rod precursors faster than the
620 triggering of the MG-dependent injury response. In this context, rod precursors form a
621 pool of cells at the base of the outer nuclear layer and proliferate as early as 16 hours
622 post-light lesion [28,82,83]. Since the already available pool of rod precursors would be
623 *gfap*:mCherry-negative, we might have missed the derived rod progeny, given our
624 sorting strategy. In summary, we show that in the light-lesioned retina, zebrafish MG
625 go through an inflammatory-like state before generating hybrid MG/RPCs that
626 eventually cycle-back to non-reactive MG as well generate neurogenic RPCs. The
627 neurogenic RPCs progressively restrict their competence to produce neurons that
628 include retinal ganglion cells first and bipolar cell last up to 6 dpl. Our study is the first
629 comprehensive description of the molecular network underlying MG self-renewal and
630 RPC differentiation to regenerating neurons which will inform future regenerative
631 therapies to treat retinal dystrophies in humans.[84].

632

633 **MATERIALS AND METHODS**

634 **Animals**

635 Zebrafish (*Danio rerio*) were raised as previously described [85]. Adult fish (6-12 months
636 old) of either sex were used for all experiments. WT animals were in the AB genetic
637 background.

638

639 **Transgenic lines**

640 To generate the *Tg(pcna:EGFP)*, the BAC CH73-140L11, containing more than 100
641 kb of the genomic *pcna* locus, was obtained from the BACPAC resource centre. A
642 cassette containing EGFP and a polyadenylation signal was recombined at the starting
643 ATG of exon 1. First, FRTgb- neo-FRT and EGFP cassettes where amplified by PCR.
644 Then, the cassettes where amplified and merged by fusion PCR with primers carrying
645 50 nucleotides of homology of the targeting sequence. Recombineering of the BAC
646 was performed as previously described [86]. BAC DNA was purified and about 50 pg of
647 BAC DNA were injected into fertilized eggs at the one cell stage. F0 were raised and
648 incrossed. F1 were identified by visual screening for GFP expression and raised. The
649 *Tg(gfap:nls-mCherry)* line was generated as previously described [61]. In addition, to
650 the line described in Lange et al. (tud117tg), a second independent insertion was
651 isolated. This insertion displays a stronger expression in MG and was hence used for
652 this study.

653

654 **Light injury**

655 WT AB and *Tg(pcna:EGFP);Tg(gfap:nls-mCherry)* fish were dark adapted for 3 days.
656 Afterwards, diffuse light lesion was performed as previously described [22]. Briefly, up to
657 4 fish were placed in a beaker filled with system water (300 ml), positioned 3 cm away

658 from the light bulb of a metal halide lamp (EXFO X-Cite 120W, EXFO Photonic
659 Solutions, Mississauga, Ontario, Canada). Fish were exposed for 30 min to a bright
660 light (≥ 100.000 lux), and then put back to system tanks in normal light conditions.
661 Uninjured fish controls were dark adapted and processed in parallel to light injured
662 animals.

663

664 **Dissociation of retinae to a single cell suspension**

665 Uninjured and light-lesioned *Tg(pcna:EGFP);Tg(gfap:nls-mCherry)* fish were exposed
666 to an overdose (0.2%) of MS-222 (Sigma) [85] until cessation of the operculum
667 movement. Subsequently, each cornea was poked with a needle, and tweezers were
668 gently pressured on each side of the eye to remove the lens. Then, tweezers were
669 used to carefully isolate the retinae, which were put in a dissociation solution of papain
670 (16 U/ml), dispase (0.2 U/ml) and DNAse (168 U/ml) dissolved in Earle's Balanced Salt
671 Solution (EBSS, Worthington Biochemical Corporation). Up to 6 retinae were put in 1.7
672 ml of dissociation solution. Retinae were digested for 30 minutes at 28°C, and then
673 calcein blue (final concentration: 1μM, Invitrogen) was added for 10 minutes to the
674 digestion solution at 28°C to stain for living cells. At the end of the enzymatic digestion,
675 mechanical trituration was applied using fire-polished glass pipettes of decreasing tip
676 diameter to help tissue dissociation. Single cells were centrifuged (300 g) at 4°C, for 6
677 minutes. The cell pellet was re-suspended in EBSS supplemented with DNAse (100
678 U/ml) to eliminate residual, ambient DNA, and albumin ovomucoid inhibitor (1:10 of
679 stock solution, Worthington Biochemical Corporation) to stop papain action. The single
680 cell solution was eventually filtered (20 μm filters) to remove clumps and debris, and
681 put on ice, ready for Fluorescent Activated Cell Sorting (FACS). Each single cell
682 suspension was obtained by pooling 8 retinae (from 4 fish, 2 males and 2 females) of

683 uninjured and light-lesioned *Tg(pcna:EGFP);Tg(gfap:mCherry)* animals. Uninjured WT
684 AB, *Tg(gfap:mCherry)* and *Tg(pcna:EGFP)* fish were used to prepare single cell
685 suspensions of dissected retinae for setting the single fluorophore gates in flow
686 cytometry. Additionally, a calcein only stained single cell suspension was prepared
687 from uninjured WT AB fish retinae for the setting of the calcein gate in the flow
688 cytometry.

689

690 **Flow cytometry and FACS**

691 A BD FACSAria™ III cell sorter was used for flow cytometry and FACS. mCherry
692 fluorophore was detected using a 561 nm excitation laser and a 610/20 nm band pass
693 filter, EGFP using a 488 nm laser and a 530/30 nm band pass filter and calcein blue
694 using a 405 nm laser and a 450/40 nm band pass filter. The gating strategy is shown
695 in the supplemental method figure for uninjured samples and was the same for all the
696 light-lesioned samples. Forward and side scatters were used to gate cells among all
697 the events in the single cell suspension and to gate singlets among those cells
698 (supplemental method figure A). mCherry-positive only as well as EGFP-positive only
699 gates were set in comparison to the unstained, WT control (supplemental method
700 figure B). Calcein blue positive, single cells were eventually gated as living cells
701 (60.000 living cells from uninjured, 44 hpl and 4 dpl samples, 41.389 living cells from
702 6 dpl sample). 15.000 cells were sorted from each samples, put on ice and sent to the
703 CMCB Deep Sequencing Facility for single cell RNA sequencing (scRNAseq).

704

705 **(Droplet based) single cell transcriptomics**

706 Single cell transcriptome sequencing was performed based on the 10x Genomics
707 Single cell transcriptome workflow [87]. Specifically, 15.000 FACS-sorted cells were
708 recovered in BSA-coated tubes containing 5 ul PBS with 0.04% BSA. Cell samples
709 were carefully mixed with Reverse Transcription Reagent (Chromium Single Cell 3'
710 Library Kit v3) and loaded onto a Chromium Single Cell B Chip to reach a recovery of
711 10.000 cells per sample. The samples were processed further following the guidelines
712 of the 10x Genomics user manual for single cell 3' RNA-seq v3. In short, the droplets
713 were directly subjected to reverse transcription, the emulsion was broken and cDNA
714 was purified using silane beads (Chromium Single Cell 3' Gel Bead Kit v2). After
715 amplification of cDNA with 11 cycles, samples were purified with 0.6x volume of SPRI
716 select beads to deplete DNA fragments smaller than 400 base pairs and cDNA quality
717 was monitored using the Agilent FragmentAnalyzer 5200 (NGS Fragment Kit). 10 ul of
718 the resulting cDNA were used to prepare single cell RNA seq libraries - involving
719 fragmentation, dA-Tailing, adapter ligation and 11 cycles of indexing PCR following
720 manufacturer's guidelines. After quantification, both libraries were sequenced on an
721 Illumina NextSeq500 in 75 base pair paired-end mode, generating 45-109 million
722 fragments per transcriptome library. The raw sequencing data was processed with the
723 'count' command of the Cell Ranger software (v2.1.0) provided by 10X Genomics. To
724 build the reference, the zebrafish genome (GRCz11) as well as gene annotation
725 (Ensembl 90) were downloaded from Ensembl and the annotation was filtered with the
726 'mkgtf' command of Cell Ranger (options: '—e attribute=gene_biotype:protein_coding
727 --attribute=gene_biotype:lincRNA –attribute=gene_biotype:antisense'). Genome
728 sequence and filtered annotation were then used as input to the 'mkref' command of
729 Cell Ranger to build the appropriate Cell Ranger.

730

731 **Bioinformatic analysis**

732 The complete software stack for the analysis is available as a Singularity container
733 (https://gitlab.hrz.tu-chemnitz.de/dcgc-bfx/singularity/singularity-single-cell, tag
734 1f5da0b). The count matrices generated with Cell Ranger were further analysed using
735 scanpy 1.8.2 (https://genomebiology.biomedcentral.com/articles/10.1186/s13059-
736 017-1382-0). For quality control, we removed cells with less than 2.000 counts, less
737 than 500 detected genes, more than 15% mitochondrial reads or more than 60% of the
738 counts in the top 50 highest expressed genes. The counts were normalised with the
739 size factors computed with calculateSumFactors from scran 1.18.5 (min.mean=0.1)[88].
740 The normalised counts were log-transformed using the numpy function log1p. The top
741 4000 highly variable genes were detected using the scanpy function
742 scanpy.pp.highly_variable_genes (n_top_genes= 4000). Cell cycle scores were
743 computed using scanpy.tl.score_genes_cell_cycle on each sample separately. As
744 genes associated to S-phase, the genes *mcm5*, *pcna*, *tyms*, *fen1*, *mcm2*, *mcm4*, *rrm1*,
745 *unga*, *gins2*, *mcm6*, *cdca7a*, *dtl*, *prim1*, *uhrf1*, *si:dkey-185e18.7*, *hells*, *rfc2*, *rpa2*, *nasp*,
746 *rad51ap1*, *gmnn*, *wdr76*, *slbp*, *ccne2*, *ubr7*, *pold3*, *msh2*, *atad2*, *rad51*, *rrm2*, *cdc45*,
747 *cdc6*, *exo1*, *tipin*, *dscc1*, *blm*, *casp8ap2*, *usp1*, *pola1*, *chaf1b*, *brip1* and *e2f8* were
748 used. As genes associated to G2/M phase, the genes *hmgb2a*, *cdk1*, *nusap1*, *ube2c*,
749 *birc5a*, *tpx2*, *top2a*, *ndc80*, *cks2*, *nuf2*, *cks1b*, *mki67*, *tmpoa*, *cenpf*, *tacc3*, *smc4*,
750 *ccnb2*, *ckap2l*, *aurkb*, *bub1*, *kif11*, *anp32e*, *tubb4b*, *gtse1*, *kif20ba*, *si:ch211-69g19.2*,
751 *jpt1a*, *cdc20*, *ttk*, *kif2c*, *rangap1a*, *ncapd2*, *dlgap5*, *si:ch211-244o22.2*, *cdca8*, *ect2*,
752 *kif23*, *hmmr*, *aurka*, *anln*, *lbr*, *ckap5*, *cenpe*, *ctcf*, *nek2*, *g2e3*, *gas2l3*, *cbx5* and *selenoh*
753 were used. A principal component analysis (PCA) was performed on the highly variable
754 genes (function scanpy.pp.pca using svd_solver='arpack'). A k-nearest-neighbour
755 (knn) graph was computed using scanpy.pp.neighbors and a UMAP was computed
756 using scanpy.tl.umap. Clustering was performed with scnapy.tl.leiden (resolution=

757 0.01). For the three resulting clusters, marker genes were computed using
758 scanpy.tl.rank_genes_groups. Two smaller clusters identified as microglia and low-
759 quality cells were removed from the downstream analysis. Detection of highly variable
760 genes PCA were performed as above on the remaining cells. A new knn graph was
761 computed (this time with n_neighbors= 50) and a new UMAP was computed.
762 Embedding densities were computed using scanpy.tl.embedding_density. Clustering
763 was performed in multiple steps, always using scanpy.tl.leiden: First, the data were
764 clustered with the resolution parameter set to 0.45. Next, cluster 10 was subclustered
765 with resolution 0.1 and cluster 0 was subclustered with resolution 0.2. Marker genes
766 of the resulting 15 clusters were computed with scanpy.tl.rank_genes_groups.
767 Differential expression analysis of pairs of clusters was performed by subsetting the
768 data to cells from those two clusters and computing differentially expressed genes with
769 scanpy.tl.rank_genes_groups. The source code for the analysis is available upon
770 reasonable request.

771

772 **Cluster annotation**

773 Cluster annotation was performed in several steps. Initially, we identified clusters by
774 considering the top 100 upregulated genes per cluster, the time point at which they
775 appeared and their cell cycle profile. Genes were manually annotated by consulting
776 the ZFIN database (http://zfin.org/) and Pubmed (https://pubmed.ncbi.nlm.nih.gov/)
777 indexed literature about retina development and regeneration. In particular, we took as
778 a reference the single cell RNA sequencing dataset of the regenerating zebrafish retina
779 from Hoang et al., 2020, for marker genes lists. Following the initial identification of cell
780 clusters, we proceeded with a finer characterization by considering differential gene
781 expression analysis for clusters that shared a similar identity. Occasionally (e.g., in the

782 case of horizontal cell precursor marker *ptf1a*), we plotted the UMAP profile of known
783 candidates from retina development or regeneration. Selected marker genes were then
784 checked for expression in the retina tissue via *in situ* hybridization, fluorescent *in situ*
785 hybridization and immunohistochemistry on cryosections.

786

787 **Tissue preparation and cutting**

788 Fish heads were fixed with 4% paraformaldehyde in 0.1 M phosphate buffer (PB, pH:
789 7.4) overnight, at 4°C. Subsequently, fixed heads where decalcified and cryoprotected
790 in 20% EDTA and 20% sucrose in 0.1M PB (pH: 7.5) overnight, at 4°C. Heads were
791 eventually embedded in 7.5% gelatin, 20% sucrose in 0.1M PB and sectioned (12 or
792 14 µm) at the cryostat (CryoStar Nx70, Thermo Scientific). Cryosections were stored
793 at -20°C.

794

795 ***in situ* hybridization probe synthesis**

796 For the synthesis of *in situ* hybridization RNA probes, 4 dpl retinae were dissected and
797 sonicated at 4°C to homogenate the tissue and to extract total RNA. We chose 4 dpl
798 samples, because transcripts of interest were enriched at 4 dpl. RNA was extracted
799 using the total RNA purification kit and following manufacturer's instructions (Norgen
800 Biotek Corporation). cDNA was then transcribed using the first strand cDNA synthesis
801 kit (Roche), followed by PCR to amplify the fragments of interest using primer pairs
802 listed in the key resource table. The amplicon was subsequently purified (gel and DNA
803 recovery kit, Zymo Research) and cloned in a TOPO TA® vector (Thermo Fisher), with
804 which competent *E coli* bacteria were transformed and cultured on Petri dishes coated
805 with agar and ampicillin, overnight at 37°C. The next day, colonies were picked up and

806 cultured in LB medium supplemented with ampicillin (1:2000) overnight at 37°C,
807 shaking, to enrich cultures for mini-prep (Gene Jet Plasmid Miniprep kit k0503, Thermo
808 Fisher). Purified plasmids were sent for sequencing (Eurofins) to verify the sequence.
809 Insert-positive colonies were further enriched in LB/ampicillin cultures for midi-prep
810 (Nucleo Bond® Xtra Midi, Macherey – Nagel) and purified plasmids were linearized to
811 transcribe anti-sense, digoxigenin labelled (DIG) RNA probes, which were stored in
812 hybridization buffer at -20°C. Probes for *her 4.1*, *crlf1a*, *hmgb2b*, *onecut1*, *onecut2*
813 were transcribed from a TOPO TA® cloned insert. Instead, the *id1* probe was
814 transcribed directly from the PCR – amplified cDNA using SP6-conjugated forward and
815 T7-conjugated reverse primers (key resource table).

816

817 ***in situ* hybridization**

818 *in situ* hybridization and fluorescent i*n situ* hybridization were performed on three
819 animals per injured time point and on three uninjured controls processed in parallel.
820 Cryosections were dried for 30 minutes at room temperature, then washed two times
821 for 10 minutes in phosphate buffer saline supplemented with 0.3% Triton X-100
822 (PBSTx) for permeabilization. *in situ* hybridization probes were denatured by warming
823 up at 70°C for 10 minutes and brief vortexing. Permeabilized sections were incubated
824 overnight in denatured probes at 62°C. The next day, sections were rinsed three times
825 (once for 15 minutes, followed by two washes of 30 minutes each) in washing buffer
826 (refer to key resource table) at 62°C. Then, in the case of chromogenic *in situ*
827 hybridization, sections were washed twice in MABT (key resource table) for 30 minutes
828 each and incubated with 2% digoxigenin blocking reagent (key resource table) in
829 MABT for 1 hour at room temperature. In the case of fluorescent *in situ* hybridization,
830 sections were washed in TNT buffer (key resource table), and then incubated with 2%

831 digoxigenin blocking reagent dissolved in TNT buffer. After, sections were incubated
832 with the AP-conjugated, anti-digoxigenin antibody (chromogenic *in situ* hybridization,
833 1:2000, key resource table) or with the POD-conjugated, anti-digoxigenin antibody
834 (fluorescent *in situ* hybridization, 1:2000, key resource table) overnight, at 4°C. The
835 next day, sections were washed four times for 20 minutes each in MABT (chromogenic
836 *in situ* hybridization) or three times for 10 minutes each in TNT buffer (fluorescent *in*
837 *situ* hybridization) at room temperature. Then, sections for chromogenic *in situ*
838 hybridization were washed for 5 minutes in staining buffer (key resource table) and
839 eventually incubated with 20 µl/ml NBT/BCIP stock solution in staining buffer, at room
840 temperature, to develop the colour reaction. Time of incubation varied between three
841 hours and overnight, depending on the target mRNA and probe concentration. In the
842 case of fluorescent *in situ* hybridization, after TNT washing steps, sections were
843 incubated for 30 minutes with 1:200 Cy3-Tyramide in TSA amplification buffer (Akoya
844 Biosciences®), at room temperature. Finally, sections from chromogenic *in situ*
845 hybridization were washed three times with PBS, for 10 minutes each and mounted in
846 70% glycerol in PBS, ready for bright field microscopy. Fluorescent *in situ* hybridization
847 sections were rinsed three times in PBS, for 10 minutes each, and then incubation with
848 primary antibody for immunohistochemistry was performed as described below.

849

850 **Immunohistochemistry**

851 Immunohistochemistry was conducted as previously described [89,90]. Sections were
852 dried at room temperature for 30 minutes and washed 3 times in PBSTx for 10 minutes
853 each. Then, primary antibodies diluted in PBSTx were applied overnight at 4°C (refer
854 to the key resource table for primary antibody host, antigen specificity and dilution).
855 For proliferating cell nuclear antigen (PCNA) retrieval, sections were immersed in 10

856 mM sodium citrate (pH: 6) for 6 minutes at a temperature higher than 80°C, then
857 washed, and finally primary anti-PCNA antibody was applied. After primary antibody
858 incubation, sections were washed three times in PBSTx for 10 minutes each, then
859 Alexa® fluorophore conjugated, secondary antibodies diluted In PBSTx were applied
860 accordingly (refer to key resource table for secondary antibody host, primary antibody
861 specificity and dilution) for 2 hours at room temperature. Sections were eventually
862 washed three times in PBS, mounted in 70% glycerol in PBS, and stored at 4°C. Each
863 staining was performed on three fish per time point upon injury and on three uninjured
864 fish controls processed in parallel. When combined with fluorescent *in situ*
865 hybridization, immunohistochemistry followed fluorescent *in situ* hybridization
866 processed sections.

867

868 **Microscopy**

869 Bright field images of chromogenic *in situ* hybridizations and fluorescent images in
870 supplemental figure 2 were acquired with the Widefield ApoTome microscope (Zeiss
871 Axio Imager.Z1) using the 20x/0.8 Plan-Apochromat, Air, DIC objective. Fluorescent
872 images in supplemental figure 1, and in Figure 4 and 6 were acquired with the laser
873 scanning confocal microscope 780 (Zeiss Axio Imager.Z1) using the 40x/1.2 C-
874 Apochromat, Water, DIC, Zeiss (supplemental figure 1 and Figure 4) and the 20x/0.8
875 Plan-Apochromat, Air, DIC, Zeiss (Figure 6). Fluorescent channels were acquired
876 sequentially to minimize crosstalk in multicolour specimens.

877

878 **Image acquisition and processing**

879 Bright field microscope images were processed with the Zeiss ZEN blue, V 2012
880 software. The extended depth of focus function (contrast method) was applied to raw,
881 bright field images of *her4.1*, *hmgb2b*, *atoh7* and *onecut1 in situ* hybridizations to
882 project the chromogenic signal of the optical stack to a single plane. Fluorescent
883 microscope images were processed using Fiji [91] for image contrast adjustments, crop
884 and rotation. Adobe Illustrator CC 2015.3 was used to assemble figures. Excel 2016
885 (Microsoft) was used to generate the plot in supplemental figure 6.

886

887 **STATISTICS**

888 Marker genes were ranked by their test statistic computed with a t-test for each gene,
889 comparing cells within the cluster to the cells outside the cluster, as implemented in
890 the scanpy function tl.rank_genes_groups. The same was done to identify differentially
891 expressed genes between pairs of clusters.

892

893 **ETHICAL STATEMENT**

894 Fish were kept according to FELASA guidelines [92]. All animal experiments were
895 conducted according to the guidelines and under supervision of the
896 Regierungspräsidium Dresden (permit: TVV 44/2017). All efforts were made to
897 minimize animal suffering and the number of animals used.

898

899 **Data availability**

900 All sequencing data that support the findings of this study have been deposited at
901 https://singlecell.broadinstitute.org/single_cell/reviewer_access/5a29ec20-d572-
902 4461-bfd3-cb8973c05f33 and are accessible through BioProject ID SCP1973.

903

904 **Acknowledgements**

905 We thank Dr. Judith Konantz, M. Fischer, S. Kunadt and D. Mögel for excellent
906 zebrafish care. We thank Katja Bernhardt for the excellent technical assistance in flow
907 cytometry and cell sorting. We would like to thank also Susanne Reinhardt and Dr.
908 Andreas Petzold from the DRESDEN-concept Genome Center for support with initial
909 planning and bioinformatic processing of the scRNAseq experiment, respectively. We
910 thank Prof. Marius Ader, Prof. Mike O. Karl, Dr. Volker Kroehne, Juliane Hammer and
911 Elisa Nerli for critically reading the manuscript. In addition, we thank the members of
912 the Brand laboratory for continued support and discussions as well as helpful
913 comments on the manuscript. We thank also Dr. Christian Lange, Dr. Robert Münch
914 and Dr. Steffen Rulands for excellent scientific discussion. This work was supported
915 by grants to M.B. from the Deutsche Forschungsgemeinschaft (BR 1746/11-1), the
916 European Union (European Research Council AdG Zf-BrainReg) and the German
917 Excellence Initiative (Wissenschaftsrat and Deutsche Forschungsgemeinschaft) (EXC
918 168). Work was supported by the DRESDEN-concept Genome Center, the Light
919 Microscopy Facility and Flow Cytometry Facility, core facilities of the CMCB at the
920 Technische Universität Dresden. The funders had no role in study design, data
921 collection and analysis, decision to publish, or preparation of the manuscript.

922

923 **Author contributions**

Conceptualization: L.C, F.R., A.W., S.H., M.B.; Investigation: L.C., F.R., A.M., J.B., A.D.; Writing - original draft: L.C., S.H., M.B.; Writing - review & editing: L.C., F.R., A.M., J.B., A.D., A.W., S.H., and M.B.; Supervision: M.B.; Funding acquisition: M.B.

REFERENCES

1. Dowling, J.E. (1987). The Retina: An Approachable Part of the Brain (Harvard University Press).
2. Amini, R., Rocha-Martins, M., and Norden, C. (2018). Neuronal Migration and Lamination in the Vertebrate Retina. Front. Neurosci. *11*, 742. 10.3389/fnins.2017.00742.
3. Hoon, M., Okawa, H., Santina, L.D., and Wong, R.O.L. (2014). Functional Architecture of the Retina: Development and Disease. Prog Retin Eye Res *42*, 44–84. 10.1016/j.preteyeres.2014.06.003.
4. Stenkamp, D.L. (2015). Development of the Vertebrate Eye and Retina. Prog Mol Biol Transl Sci *134*, 397–414. 10.1016/bs.pmbts.2015.06.006.
5. Agathocleous, M., and Harris, W.A. (2009). From progenitors to differentiated cells in the vertebrate retina. Annu Rev Cell Dev Biol *25*, 45–69. 10.1146/annurev.cellbio.042308.113259.
6. Alexiades, M.R., and Cepko, C.L. (1997). Subsets of retinal progenitors display temporally regulated and distinct biases in the fates of their progeny. Development *124*, 1119–1131. 10.1242/dev.124.6.1119.
7. Cepko, C. (2014). Intrinsically different retinal progenitor cells produce specific types of progeny. Nat Rev Neurosci *15*, 615–627. 10.1038/nrn3767.
8. Cepko, C.L., Austin, C.P., Yang, X., Alexiades, M., and Ezzeddine, D. (1996). Cell fate determination in the vertebrate retina. PNAS *93*, 589–595. 10.1073/pnas.93.2.589.
9. Livesey, F.J., and Cepko, C.L. (2001). Vertebrate neural cell-fate determination: lessons from the retina. Nat Rev Neurosci *2*, 109–118. 10.1038/35053522.
10. Stenkamp, D.L. (2007). Neurogenesis in the fish retina. Int Rev Cytol *259*, 173–224. 10.1016/S0074-7696(06)59005-9.
11. Turner, D.L., and Cepko, C.L. (1987). A common progenitor for neurons and glia persists in rat retina late in development. Nature *328*, 131–136. 10.1038/328131a0.
12. Weber, I.P., Ramos, A.P., Strzyz, P.J., Leung, L.C., Young, S., and Norden, C. (2014). Mitotic Position and Morphology of Committed Precursor Cells in the Zebrafish Retina Adapt to Architectural Changes upon Tissue Maturation. Cell Reports *7*, 386–397. 10.1016/j.celrep.2014.03.014.
13. Young, R.W. (1985). Cell differentiation in the retina of the mouse. Anat Rec *212*, 199–205. 10.1002/ar.1092120215.
14. Fleisch, V.C., Fraser, B., and Allison, W.T. (2011). Investigating regeneration and functional integration of CNS neurons: Lessons from zebrafish genetics and other fish species. Biochimica et Biophysica Acta (BBA) - Molecular Basis of Disease *1812*, 364–380. 10.1016/j.bbadis.2010.10.012.
15. Saade, C.J., Alvarez-Delfin, K., and Fadool, J.M. (2013). Rod photoreceptors protect from cone degeneration-induced retinal remodeling and restore visual responses in zebrafish. J Neurosci *33*, 1804–1814. 10.1523/JNEUROSCI.2910-12.2013.
16. Bernardos, R.L., Barthel, L.K., Meyers, J.R., and Raymond, P.A. (2007). Late-Stage Neuronal Progenitors in the Retina Are Radial Muller Glia That Function as Retinal Stem Cells. Journal of Neuroscience *27*, 7028–7040. 10.1523/JNEUROSCI.1624-07.2007.
17. Fimbel, S.M., Montgomery, J.E., Burket, C.T., and Hyde, D.R. (2007). Regeneration of Inner Retinal Neurons after Intravitreal Injection of Ouabain in

Zebrafish. Journal of Neuroscience *27*, 1712–1724. 10.1523/JNEUROSCI.5317-06.2007.
18. Powell, C., Cornblath, E., Elsaeidi, F., Wan, J., and Goldman, D. (2016). Zebrafish Müller glia-derived progenitors are multipotent, exhibit proliferative biases and regenerate excess neurons. Sci Rep *6*, 24851. 10.1038/srep24851.
19. Sherpa, T., Fimbel, S.M., Mallory, D.E., Maaswinkel, H., Spritzer, S.D., Sand, J.A., Li, L., Hyde, D.R., and Stenkamp, D.L. (2008). Ganglion cell regeneration following whole-retina destruction in zebrafish. Devel Neurobio *68*, 166–181. 10.1002/dneu.20568.
20. Vihtelic, T.S., Soverly, J.E., Kassen, S.C., and Hyde, D.R. (2006). Retinal regional differences in photoreceptor cell death and regeneration in light-lesioned albino zebrafish. Experimental Eye Research *82*, 558–575. 10.1016/j.exer.2005.08.015.
21. Vihtelic, T.S., and Hyde, D.R. (2000). Light-induced rod and cone cell death and regeneration in the adult albino zebrafish (Danio rerio) retina. J Neurobiol *44*, 289–307. 10.1002/1097-4695(20000905)44:3<289::aid-neu1>3.0.co;2-h.
22. Weber, A., Hochmann, S., Cimalla, P., Gärtner, M., Kuscha, V., Hans, S., Geffarth, M., Kaslin, J., Koch, E., and Brand, M. (2013). Characterization of light lesion paradigms and optical coherence tomography as tools to study adult retina regeneration in zebrafish. PLoS One *8*, e80483. 10.1371/journal.pone.0080483.
23. Gorsuch, R.A., and Hyde, D.R. (2014). Regulation of Müller glial dependent neuronal regeneration in the damaged adult zebrafish retina. Experimental Eye Research *123*, 131–140. 10.1016/j.exer.2013.07.012.
24. Lahne, M., Nagashima, M., Hyde, D.R., and Hitchcock, P.F. (2020). Reprogramming Müller Glia to Regenerate Retinal Neurons. Annu Rev Vis Sci *6*, 171–193. 10.1146/annurev-vision-121219-081808.
25. Lenkowski, J.R., and Raymond, P.A. (2014). Müller glia: Stem cells for generation and regeneration of retinal neurons in teleost fish. Progress in Retinal and Eye Research *40*, 94–123. 10.1016/j.preteyeres.2013.12.007.
26. Wan, J., and Goldman, D. (2016). Retina regeneration in zebrafish. Curr Opin Genet Dev *40*, 41–47. 10.1016/j.gde.2016.05.009.
27. Nagashima, M., Barthel, L.K., and Raymond, P.A. (2013). A self-renewing division of zebrafish Müller glial cells generates neuronal progenitors that require N-cadherin to regenerate retinal neurons. Development *140*, 4510–4521. 10.1242/dev.090738.
28. Thummel, R., Kassen, S.C., Enright, J.M., Nelson, C.M., Montgomery, J.E., and Hyde, D.R. (2008). Characterization of Müller glia and neuronal progenitors during adult zebrafish retinal regeneration. Experimental Eye Research *87*, 433–444. 10.1016/j.exer.2008.07.009.
29. Fausett, B.V., and Goldman, D. (2006). A Role for 1 Tubulin-Expressing Muller Glia in Regeneration of the Injured Zebrafish Retina. Journal of Neuroscience *26*, 6303–6313. 10.1523/JNEUROSCI.0332-06.2006.
30. Fausett, B.V., Gumerson, J.D., and Goldman, D. (2008). The Proneural Basic Helix-Loop-Helix Gene Ascl1a Is Required for Retina Regeneration. Journal of Neuroscience *28*, 1109–1117. 10.1523/JNEUROSCI.4853-07.2008.
31. Ramachandran, R., Zhao, X.-F., and Goldman, D. (2011). Ascl1a/Dkk/ -catenin signaling pathway is necessary and glycogen synthase kinase-3 inhibition is sufficient for zebrafish retina regeneration. Proceedings of the National Academy of Sciences *108*, 15858–15863. 10.1073/pnas.1107220108.

32. Nelson, C.M., Ackerman, K.M., O'Hayer, P., Bailey, T.J., Gorsuch, R.A., and Hyde, D.R. (2013). Tumor Necrosis Factor-Alpha Is Produced by Dying Retinal Neurons and Is Required for Muller Glia Proliferation during Zebrafish Retinal Regeneration. Journal of Neuroscience *33*, 6524–6539. 10.1523/JNEUROSCI.3838-12.2013.
33. Ramachandran, R., Reifler, A., Parent, J.M., and Goldman, D. (2010). Conditional gene expression and lineage tracing of tuba1a expressing cells during zebrafish development and retina regeneration. J. Comp. Neurol. *518*, 4196–4212. 10.1002/cne.22448.
34. Thummel, R., Enright, J.M., Kassen, S.C., Montgomery, J.E., Bailey, T.J., and Hyde, D.R. (2010). Pax6a and Pax6b are required at different points in neuronal progenitor cell proliferation during zebrafish photoreceptor regeneration. Experimental Eye Research *90*, 572–582. 10.1016/j.exer.2010.02.001.
35. Wan, J., Ramachandran, R., and Goldman, D. (2012). HB-EGF Is Necessary and Sufficient for Müller Glia Dedifferentiation and Retina Regeneration. Developmental Cell *22*, 334–347. 10.1016/j.devcel.2011.11.020.
36. Zhao, X.-F., Wan, J., Powell, C., Ramachandran, R., Myers, M.G., and Goldman, D. (2014). Leptin and IL-6 family cytokines synergize to stimulate Müller glia reprogramming and retina regeneration. Cell Rep *9*, 272–284. 10.1016/j.celrep.2014.08.047.
37. Hoang, T., Wang, J., Boyd, P., Wang, F., Santiago, C., Jiang, L., Yoo, S., Lahne, M., Todd, L.J., Jia, M., et al. (2020). Gene regulatory networks controlling vertebrate retinal regeneration. Science *370*, eabb8598. 10.1126/science.abb8598.
38. Gorsuch, R.A., Lahne, M., Yarka, C.E., Petravick, M.E., Li, J., and Hyde, D.R. (2017). Sox2 regulates Müller glia reprogramming and proliferation in the regenerating zebrafish retina via Lin28 and Ascl1a. Exp Eye Res *161*, 174–192. 10.1016/j.exer.2017.05.012.
39. Raymond, P.A., Barthel, L.K., Bernardos, R.L., and Perkowski, J.J. (2006). Molecular characterization of retinal stem cells and their niches in adult zebrafish. BMC Dev Biol *6*, 36. 10.1186/1471-213X-6-36.
40. Cameron, D.A., Gentile, K.L., Middleton, F.A., and Yurco, P. (2005). Gene expression profiles of intact and regenerating zebrafish retina. Mol Vis *11*, 775–791.
41. Kassen, S.C., Ramanan, V., Montgomery, J.E., T. Burket, C., Liu, C.-G., Vihtelic, T.S., and Hyde, D.R. (2007). Time course analysis of gene expression during light-induced photoreceptor cell death and regeneration in *albino* zebrafish. Devel Neurobio *67*, 1009–1031. 10.1002/dneu.20362.
42. Kramer, A.C., Gurdziel, K., and Thummel, R. (2021). A Comparative Analysis of Gene and Protein Expression Throughout a Full 28-Day Retinal Regeneration Time-Course in Adult Zebrafish. Front Cell Dev Biol *9*, 741514. 10.3389/fcell.2021.741514.
43. Lahne, M., Brecker, M., Jones, S.E., and Hyde, D.R. (2020). The Regenerating Adult Zebrafish Retina Recapitulates Developmental Fate Specification Programs. Front Cell Dev Biol *8*, 617923. 10.3389/fcell.2020.617923.
44. Morris, A.C., Forbes-Osborne, M.A., Pillai, L.S., and Fadool, J.M. (2011). Microarray Analysis of XOPS-mCFP Zebrafish Retina Identifies Genes Associated with Rod Photoreceptor Degeneration and Regeneration. Investigative Ophthalmology & Visual Science *52*, 2255–2266. 10.1167/iovs.10-6022.

45. Ng Chi Kei, J., Currie, P.D., and Jusuf, P.R. (2017). Fate bias during neural regeneration adjusts dynamically without recapitulating developmental fate progression. Neural Dev *12*, 12. 10.1186/s13064-017-0089-y.
46. Qin, Z., Barthel, L.K., and Raymond, P.A. (2009). Genetic evidence for shared mechanisms of epimorphic regeneration in zebrafish. Proc Natl Acad Sci U S A *106*, 9310–9315. 10.1073/pnas.0811186106.
47. Ramachandran, R., Zhao, X.-F., and Goldman, D. (2012). Insm1a-mediated gene repression is essential for the formation and differentiation of Müller glia-derived progenitors in the injured retina. Nat Cell Biol *14*, 1013–1023. 10.1038/ncb2586.
48. Xu, B., Tang, X., Jin, M., Zhang, H., Du, L., Yu, S., and He, J. (2020). Unifying developmental programs for embryonic and postembryonic neurogenesis in the zebrafish retina. Development *147*, dev185660. 10.1242/dev.185660.
49. Lahne, M., Li, J., Marton, R.M., and Hyde, D.R. (2015). Actin-Cytoskeleton- and Rock-Mediated INM Are Required for Photoreceptor Regeneration in the Adult Zebrafish Retina. J. Neurosci. *35*, 15612–15634. 10.1523/JNEUROSCI.5005-14.2015.
50. Macosko, E.Z., Basu, A., Satija, R., Nemesh, J., Shekhar, K., Goldman, M., Tirosh, I., Bialas, A.R., Kamitaki, N., Martersteck, E.M., et al. (2015). Highly Parallel Genome-wide Expression Profiling of Individual Cells Using Nanoliter Droplets. Cell *161*, 1202–1214. 10.1016/j.cell.2015.05.002.
51. Tirosh, I., Izar, B., Prakadan, S.M., Wadsworth, M.H., Treacy, D., Trombetta, J.J., Rotem, A., Rodman, C., Lian, C., Murphy, G., et al. (2016). Dissecting the multicellular ecosystem of metastatic melanoma by single-cell RNA-seq. Science *352*, 189–196. 10.1126/science.aad0501.
52. Whitfield, M.L., Sherlock, G., Saldanha, A.J., Murray, J.I., Ball, C.A., Alexander, K.E., Matese, J.C., Perou, C.M., Hurt, M.M., Brown, P.O., et al. (2002). Identification of genes periodically expressed in the human cell cycle and their expression in tumors. Mol Biol Cell *13*, 1977–2000. 10.1091/mbc.02-02-0030.
53. Wu, F., Bard, J.E., Kann, J., Yergeau, D., Sapkota, D., Ge, Y., Hu, Z., Wang, J., Liu, T., and Mu, X. (2021). Single cell transcriptomics reveals lineage trajectory of retinal ganglion cells in wild-type and Atoh7-null retinas. Nat Commun *12*, 1465. 10.1038/s41467-021-21704-4.
54. Bernardos, R.L., and Raymond, P.A. (2006). GFAP transgenic zebrafish. Gene Expr Patterns *6*, 1007–1013. 10.1016/j.modgep.2006.04.006.
55. Peterson, R.E., Fadool, J.M., Mcclintock, J., and Linser, P.J. (2001). Müller cell differentiation in the zebrafish neural retina: Evidence of distinct early and late stages in cell maturation. Journal of Comparative Neurology *429*, 530–540. 10.1002/1096-9861(20010122)429:4<530::AID-CNE2>3.0.CO;2-C.
56. Yurco, P., and Cameron, D.A. (2005). Responses of Müller glia to retinal injury in adult zebrafish. Vision Research *45*, 991–1002. 10.1016/j.visres.2004.10.022.
57. D'Aniello, E., Ravisankar, P., and Waxman, J.S. (2015). Rdh10a Provides a Conserved Critical Step in the Synthesis of Retinoic Acid during Zebrafish Embryogenesis. PLOS ONE *10*, e0138588. 10.1371/journal.pone.0138588.
58. Feng, L., Hernandez, R.E., Waxman, J.S., Yelon, D., and Moens, C.B. (2010). Dhrs3a regulates retinoic acid biosynthesis through a feedback inhibition mechanism. Developmental Biology *338*, 1–14. 10.1016/j.ydbio.2009.10.029.
59. Holmes, R.S., and Hempel, J. (2011). Comparative studies of vertebrate aldehyde dehydrogenase 3: Sequences, structures, phylogeny and evolution.

Evidence for a mammalian origin for the ALDH3A1 gene. Chemico-Biological Interactions *191*, 113–121. 10.1016/j.cbi.2011.01.014.
60. Baraban, M., Anselme, I., Schneider-Maunoury, S., and Giudicelli, F. (2013). Zebrafish Embryonic Neurons Transport Messenger RNA to Axons and Growth Cones In Vivo. J. Neurosci. *33*, 15726–15734. 10.1523/JNEUROSCI.1510-13.2013.
61. Lange, C., Rost, F., Machate, A., Reinhardt, S., Lesche, M., Weber, A., Kuscha, V., Dahl, A., Rulands, S., and Brand, M. (2020). Single cell sequencing of radial glia progeny reveals diversity of newborn neurons in the adult zebrafish brain. Development, 1855951. 10.1242/dev.185595.
62. Mu, Z., Zhang, S., He, C., Hou, H., Liu, D., Hu, N., and Xu, H. (2016). Expression of SoxC Transcription Factors during Zebrafish Retinal and Optic Nerve Regeneration. Neurosci Bull *33*, 53–61. 10.1007/s12264-016-0073-2.
63. Jusuf, P.R., Almeida, A.D., Randlett, O., Joubin, K., Poggi, L., and Harris, W.A. (2011). Origin and Determination of Inhibitory Cell Lineages in the Vertebrate Retina. J. Neurosci. *31*, 2549–2562. 10.1523/JNEUROSCI.4713-10.2011.
64. Jusuf, P.R., and Harris, W.A. (2009). Ptf1a is expressed transiently in all types of amacrine cells in the embryonic zebrafish retina. Neural Dev *4*, 34. 10.1186/1749-8104-4-34.
65. Craig, S.E.L., Calinescu, A.-A., and Hitchcock, P.F. (2008). Identification of the molecular signatures integral to regenerating photoreceptors in the retina of the zebra fish. j ocul biol dis inform *1*, 73–84. 10.1007/s12177-008-9011-5.
66. Blackshaw, S., Harpavat, S., Trimarchi, J., Cai, L., Huang, H., Kuo, W.P., Weber, G., Lee, K., Fraioli, R.E., Cho, S.-H., et al. (2004). Genomic analysis of mouse retinal development. PLoS Biol *2*, E247. 10.1371/journal.pbio.0020247.
67. Silva, N.J., Nagashima, M., Li, J., Kakuk-Atkins, L., Ashrafzadeh, M., Hyde, D.R., and Hitchcock, P.F. (2020). Inflammation and matrix metalloproteinase 9 (Mmp-9) regulate photoreceptor regeneration in adult zebrafish. Glia *68*, 1445–1465. 10.1002/glia.23792.
68. Wilson, S.G., Wen, W., Pillai-Kastoori, L., and Morris, A.C. (2016). Tracking the fate of her4 expressing cells in the regenerating retina using her4:Kaede zebrafish. Exp Eye Res *145*, 75–87. 10.1016/j.exer.2015.11.002.
69. Campbell, L.J., Levendusky, J.L., Steines, S.A., and Hyde, D.R. (2022). Retinal regeneration requires dynamic Notch signaling. Neural Regen Res *17*, 1199–1209. 10.4103/1673-5374.327326.
70. Buenaventura, D.F., Ghinia-Tegla, M.G., and Emerson, M.M. (2018). Fate-restricted retinal progenitor cells adopt a molecular profile and spatial position distinct from multipotent progenitor cells. Dev Biol *443*, 35–49. 10.1016/j.ydbio.2018.06.023.
71. Corso-Díaz, X., and Simpson, E.M. (2015). Nr2e1 regulates retinal lamination and the development of Müller glia, S-cones, and glycineric amacrine cells during retinogenesis. Molecular Brain *8*, 37. 10.1186/s13041-015-0126-x.
72. Kitambi, S.S., and Hauptmann, G. (2007). The zebrafish orphan nuclear receptor genes nr2e1 and nr2e3 are expressed in developing eye and forebrain. Gene Expression Patterns *7*, 521–528. 10.1016/j.modgep.2006.10.006.
73. Muto, A., Iida, A., Satoh, S., and Watanabe, S. (2009). The group E Sox genes Sox8 and Sox9 are regulated by Notch signaling and are required for Müller glial cell development in mouse retina. Exp Eye Res *89*, 549–558. 10.1016/j.exer.2009.05.006.
74. Poché, R.A., Furuta, Y., Chaboissier, M.-C., Schedl, A., and Behringer, R.R. (2008). Sox9 is expressed in mouse multipotent retinal progenitor cells and

functions in Müller Glial cell development. Journal of Comparative Neurology *510*, 237–250. 10.1002/cne.21746.
75. Nerli, E., Kretzschmar, J., Bianucci, T., Rocha-Martins, M., Zechner, C., and Norden, C. (2022). Deterministic and probabilistic fate decisions co-exist in a single retinal lineage. 2022.08.11.503564. 10.1101/2022.08.11.503564.
76. Poggi, L., Vitorino, M., Masai, I., and Harris, W.A. (2005). Influences on neural lineage and mode of division in the zebrafish retina in vivo. J Cell Biol *171*, 991–999. 10.1083/jcb.200509098.
77. Godinho, L., Williams, P.R., Claassen, Y., Provost, E., Leach, S.D., Kamermans, M., and Wong, R.O.L. (2007). Nonapical Symmetric Divisions Underlie Horizontal Cell Layer Formation in the Developing Retina In Vivo. Neuron *56*, 597–603. 10.1016/j.neuron.2007.09.036.
78. Suzuki, S.C., Bleckert, A., Williams, P.R., Takechi, M., Kawamura, S., and Wong, R.O.L. (2013). Cone photoreceptor types in zebrafish are generated by symmetric terminal divisions of dedicated precursors. PNAS *110*, 15109–15114. 10.1073/pnas.1303551110.
79. Emerson, M.M., Surzenko, N., Goetz, J.J., Trimarchi, J., and Cepko, C.L. (2013). Otx2 and Onecut1 promote the fates of cone photoreceptors and horizontal cells and repress rod photoreceptors. Dev Cell *26*, 59–72. 10.1016/j.devcel.2013.06.005.
80. Klimova, L., Antosova, B., Kuzelova, A., Strnad, H., and Kozmik, Z. (2015). Onecut1 and Onecut2 transcription factors operate downstream of Pax6 to regulate horizontal cell development. Developmental Biology *402*, 48–60. 10.1016/j.ydbio.2015.02.023.
81. Sapkota, D., Chintala, H., Wu, F., Fliesler, S.J., Hu, Z., and Mu, X. (2014). Onecut1 and Onecut2 redundantly regulate early retinal cell fates during development. PNAS *111*, E4086–E4095. 10.1073/pnas.1405354111.
82. Morris, A.C., Schroeter, E.H., Bilotta, J., Wong, R.O.L., and Fadool, J.M. (2005). Cone survival despite rod degeneration in XOPS-mCFP transgenic zebrafish. Invest Ophthalmol Vis Sci *46*, 4762–4771. 10.1167/iovs.05-0797.
83. Stenkamp, D.L. (2011). The rod photoreceptor lineage of teleost fish. Progress in Retinal and Eye Research *30*, 395–404. 10.1016/j.preteyeres.2011.06.004.
84. Javed, A., and Cayouette, M. (2017). Temporal Progression of Retinal Progenitor Cell Identity: Implications in Cell Replacement Therapies. Frontiers in Neural Circuits *11*.
85. Nusslein-Volhard, C., and Dahm, R. (2002). Zebrafish (Oxford University Press).
86. Zhang, Y., Buchholz, F., Muyrers, J.P.P., and Stewart, A.F. (1998). A new logic for DNA engineering using recombination in Escherichia coli. Nat Genet *20*, 123–128. 10.1038/2417.
87. Zheng, G.X.Y., Terry, J.M., Belgrader, P., Ryvkin, P., Bent, Z.W., Wilson, R., Ziraldo, S.B., Wheeler, T.D., McDermott, G.P., Zhu, J., et al. (2017). Massively parallel digital transcriptional profiling of single cells. Nat Commun *8*, 14049. 10.1038/ncomms14049.
88. Lun, A.T.L., McCarthy, D.J., and Marioni, J.C. (2016). A step-by-step workflow for low-level analysis of single-cell RNA-seq data with Bioconductor. 10.12688/f1000research.9501.2.
89. Grandel, H., Kaslin, J., Ganz, J., Wenzel, I., and Brand, M. (2006). Neural stem cells and neurogenesis in the adult zebrafish brain: Origin, proliferation dynamics, migration and cell fate. Developmental Biology *295*, 263–277. 10.1016/j.ydbio.2006.03.040.

90. Kroehne, V., Freudenreich, D., Hans, S., Kaslin, J., and Brand, M. (2011). Regeneration of the adult zebrafish brain from neurogenic radial glia-type progenitors. Development *138*, 4831–4841. 10.1242/dev.072587.
91. Schindelin, J., Arganda-Carreras, I., Frise, E., Kaynig, V., Longair, M., Pietzsch, T., Preibisch, S., Rueden, C., Saalfeld, S., Schmid, B., et al. (2012). Fiji: an open-source platform for biological-image analysis. Nat Methods *9*, 676–682. 10.1038/nmeth.2019.
92. Aleström, P., D'Angelo, L., Midtlyng, P.J., Schorderet, D.F., Schulte-Merker, S., Sohm, F., and Warner, S. (2020). Zebrafish: Housing and husbandry recommendations. Lab Anim *54*, 213–224. 10.1177/0023677219869037.

Figure 1

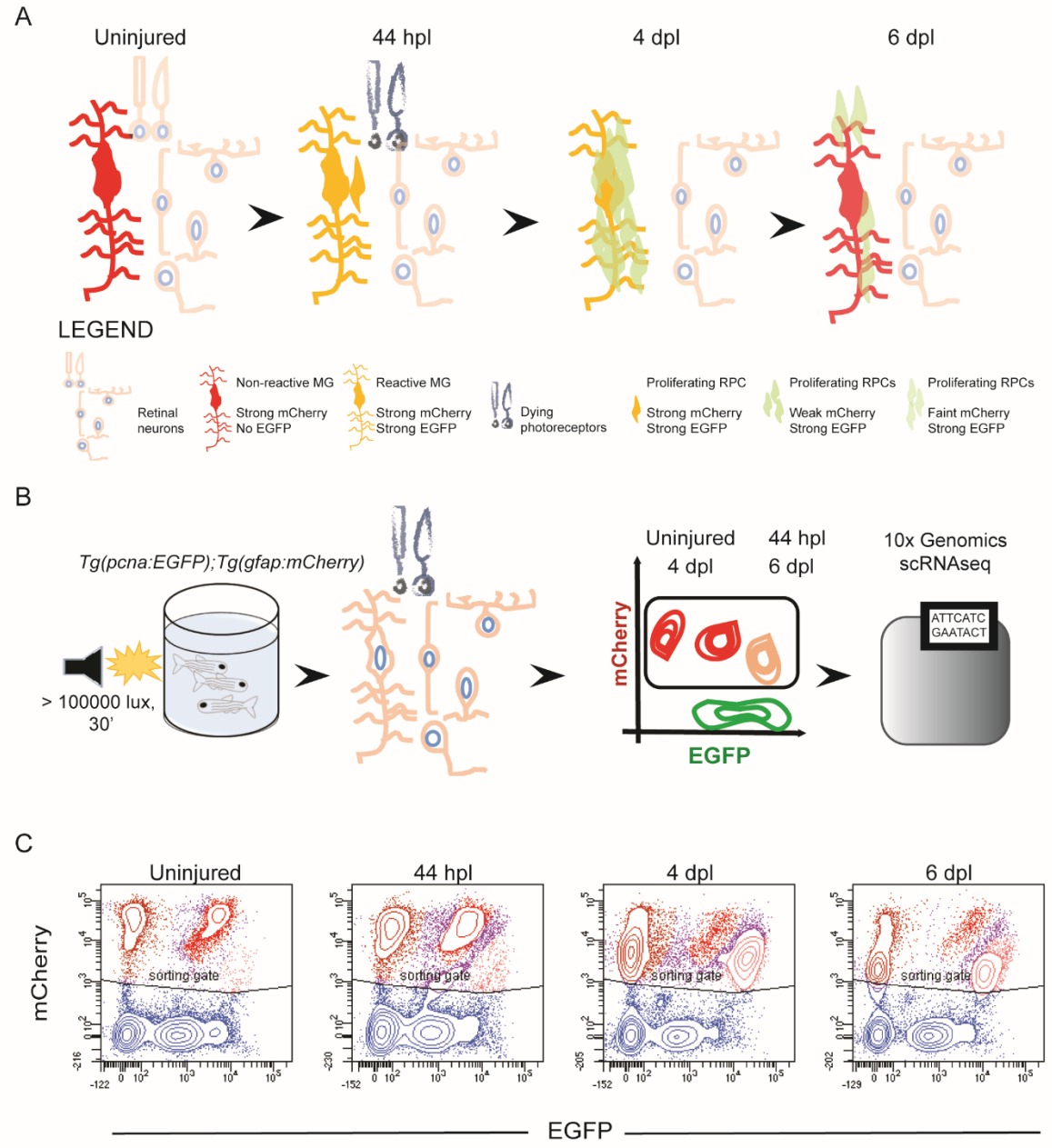
A
Uninjured
44 hpl
4 dpl
6 dpl
LEGEND
Retinal neurons
Non-reactive MG
Strong mCherry
No EGFP
Reactive MG
Strong mCherry
Strong EGFP
Dying photoreceptors
Proliferating RPC
Strong mCherry
Strong EGFP
Proliferating RPCs
Weak mCherry
Strong EGFP
Proliferating RPCs
Faint mCherry
Strong EGFP
B
Tg(pcna:EGFP);Tg(gfap:mCherry)
> 100000 lux, 30'
Uninjured
4 dpl
44 hpl
6 dpl
mCherry
EGFP
10x Genomics
scRNAseq
ATTCATC
GAATACT
C
Uninjured
44 hpl
4 dpl
6 dpl
mCherry
sorting gate
EGFP

Figure 1: Isolation of individual MG, RPCs and regenerated progeny using fluorescent reporters. (A) Schematic illustration of the rationale to isolate individual cells from regenerating retinae of double transgenic *Tg(pcna:EGFP);Tg(gfap:mCherry)* animals. In the uninjured retina, MG express strong levels of mCherry but no EGFP. Upon light lesion, which results in dying photoreceptors, MG turn on EGFP resulting in the presence of both fluorophores at 44 hours post lesion (hpl). At 4 days post lesion (dpl), MG remain to contain strong mCherry and EGFP levels. In contrast, further proliferating RPCs display weak mCherry but strong EGFP fluorescence. Finally, MG have lost the EGFP signal at 6 dpl, expressing mCherry only. RPCs, which start to migrate and differentiate, are still detectable but show diluted levels of mCherry and EGFP. **(B)** Schematic illustration of the workflow for the scRNAseq experiment. Uninjured control and light lesioned retinae (44 hpl, 4 dpl, 6 dpl) of double transgenic *Tg(pcna:EGFP);Tg(gfap:mCherry)* animals were dissociated to obtain a single cell suspension. Following fluorescent activated cell sorting of mCherry-positive only and EGFP/mCherry-double positive cells, individual cells were eventually subjected to droplet-based, 10x Genomics scRNAseq. **(C)** Flow cytometry plots depicting EGFP and mCherry fluorescence of dissociated retinal cells at the indicated time points. Cells in the sorting gate include mCherry-positive only as well as mCherry/EGFP-double positive cells.

Figure 2

A

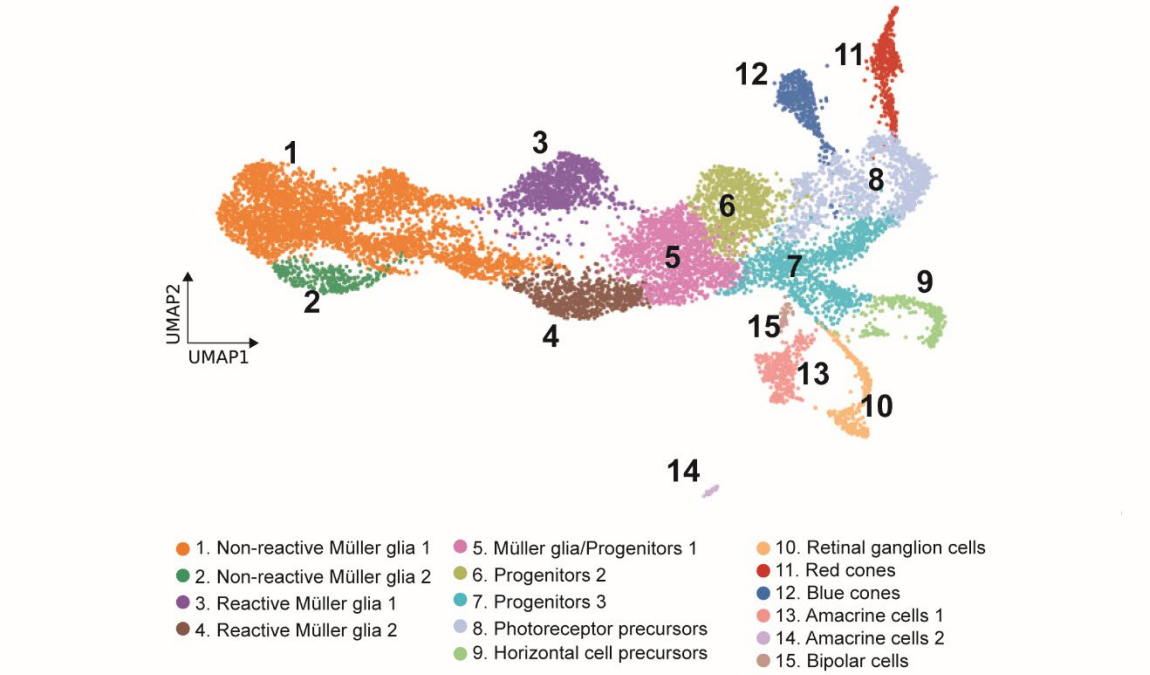

B

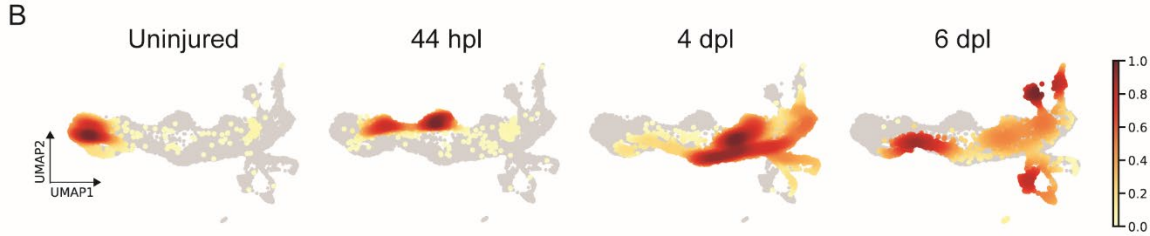

C

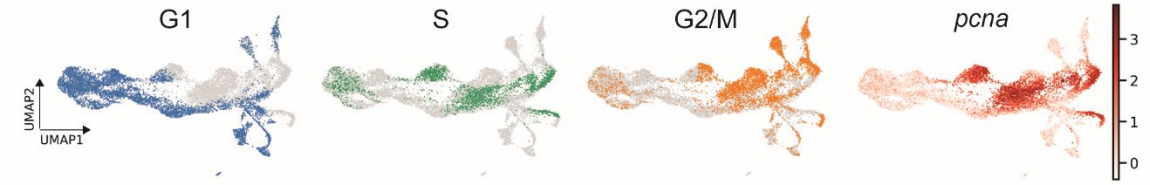

D

Figure 2: scRNAseq identifies 15 different cell populations in the light-lesioned retina. (A) 11.690 cells depicted on the uniform manifold approximation and projection (UMAP) map. From left to right, the map shows a progressive emergence of MG, RPCs and progeny clusters. See figure legend for the detailed information about cluster identity. **(B)** Normalized cell density on the UMAP for the 4 different samples (uninjured, 44 hpl, 4 and 6 dpl). Dark red shows strong cell enrichment and no color absence of cells. **(C)** Cells colored by cell cycle phases (G1, S, and G2/M phase in blue, green and orange, respectively). **(D)** Expression of *pcna*. Legend: logarithm of normalized counts per million.

Figure 3

A

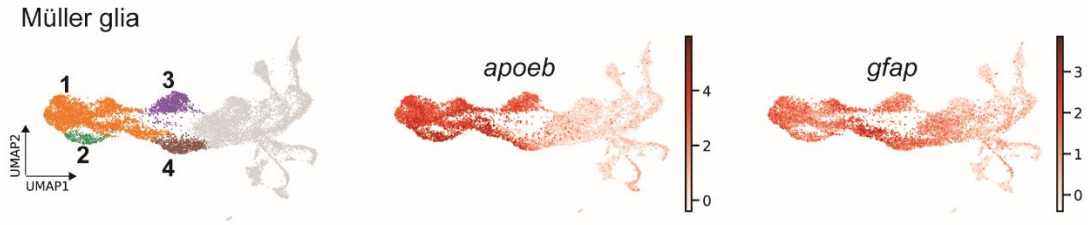

B

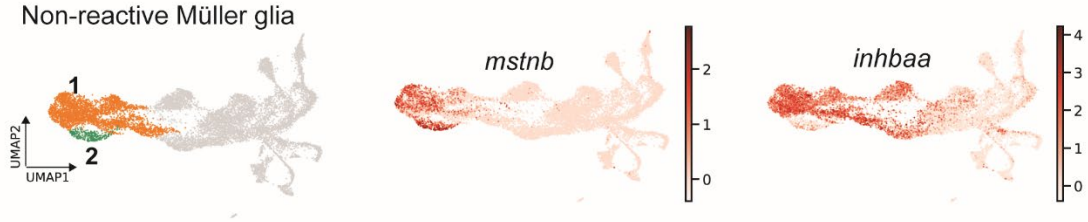

C

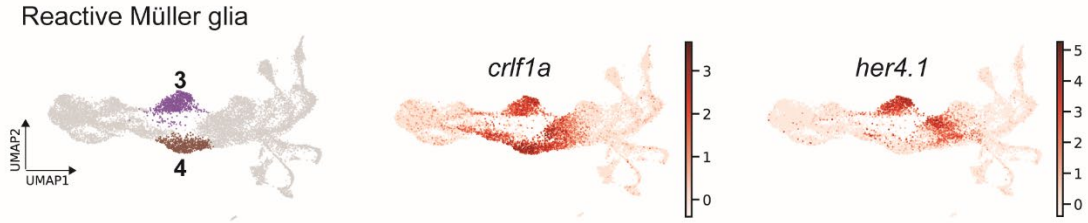

D

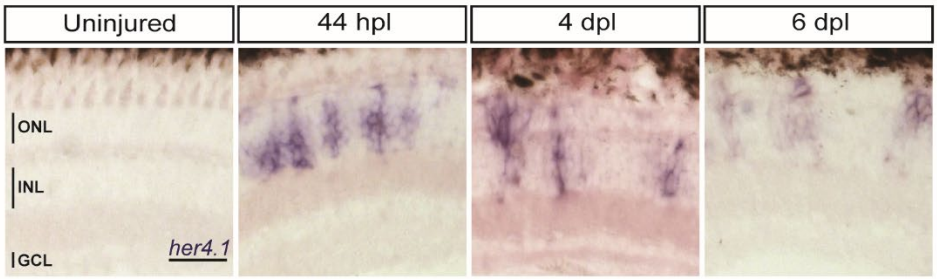

Figure 3: scRNAseq reveals heterogeneity in Müller glia and identifies two populations of non-reactive and two of reactive Müller glia in the light-lesioned retina. (A) Four Müller glia clusters (cluster 1-4) and the expression levels of *apoeb* and *gfap*. **(B)** The two non-reactive Müller glia clusters (cluster 1 and 2) and the expression levels of *mstnb* and *inhbaa*. Cells of both clusters express *mstnb*, but only cells in cluster 1 expresses *inhbaa*. **(C)** Visualization of the two reactive Müller glia clusters (cluster 3 and 4) and the relative expression levels of *crlf1a* and *her4.1* projected onto the main transcriptional UMAP. Cells of both clusters express *crlf1a*, but only cells in cluster 3 expresses *her4.1*. **(D)** Bright field microscopy images of chromogenic *in situ* hybridization detecting *her4.1* on retinal sections of uninjured control animals and at 44 hours post lesion (hpl), 4 days post lesion (dpl) and 6 dpl. The position of the outer nuclear layer (ONL), inner nuclear layer (INL) and ganglion cell layer (GCL) is indicated in the uninjured sample. Scale bar: 30 µm.

Figure 4

A

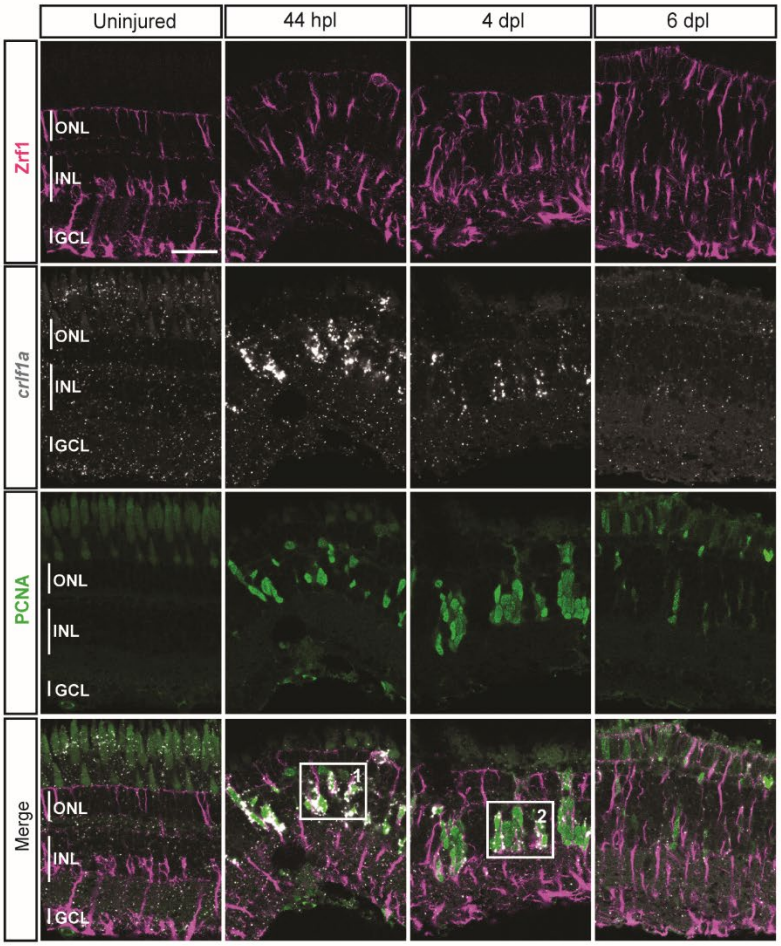
Uninjured
44 hpl
4 dpl
6 dpl
Zrf1
crlf1a
PCNA
Merge
ONL
INL
GCL
1
2

B

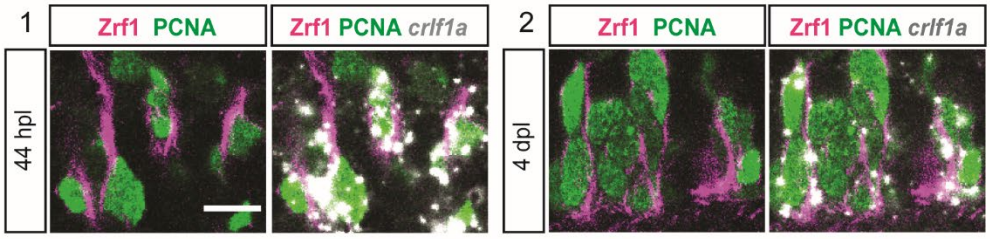
1
Zrf1 PCNA
Zrf1 PCNA crlf1a
2
Zrf1 PCNA
Zrf1 PCNA crlf1a
44 hpl
4 dpl

Figure 4: expression profile of *crlf1a* during retina regeneration. (A) Confocal images of fluorescent *in situ* hybridization for *crlf1a* (grey) and immunohistochemistry detecting Zrf1-positive MG fibers (magenta) and the proliferation marker PCNA (green) on retinal sections of uninjured control animals and at 44 hours post lesion (hpl), 4 days post lesion (dpl) and 6 dpl. The position of the outer nuclear layer (ONL), inner nuclear laser (INL) and ganglion cell layer (GCL) is indicated in the uninjured sample. Scale bar: 30 µm. **(B)** Magnification of the areas indicated by the squares 1 and 2 in panel A. Scale bar: 10 µm.

Figure 5

A

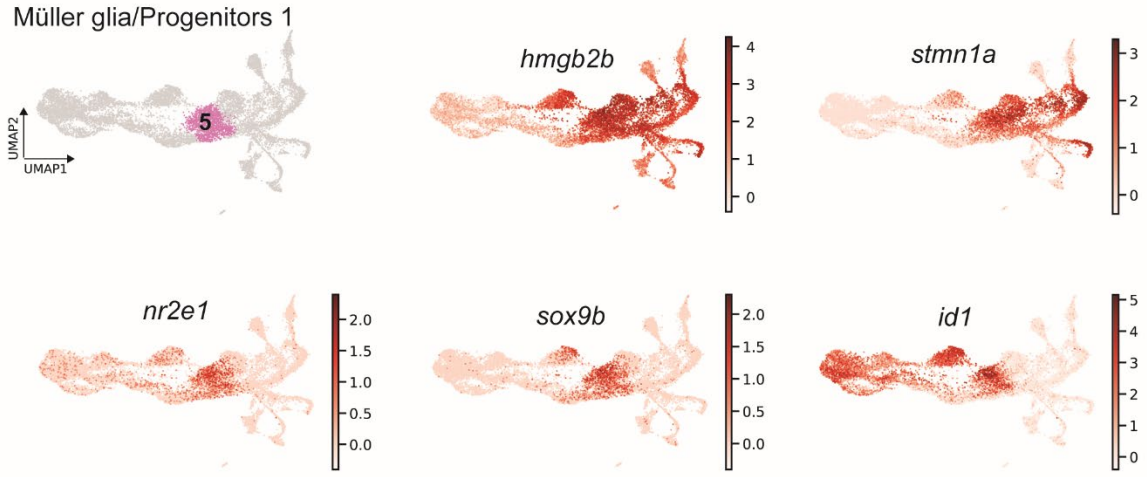
Müller glia/Progenitors 1
5
UMAP2
UMAP1
hmgb2b
stmn1a
nr2e1
sox9b
id1

B

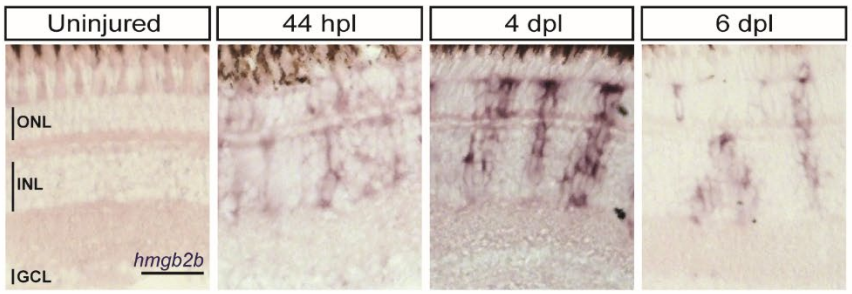
Uninjured
44 hpl
4 dpl
6 dpl
ONL
INL
GCL
hmgb2b

Figure 5: scRNAseq identifies a transient cell population with hybrid characteristics of reactive Müller glia and early progenitors in the light-lesioned retina. (A) The progenitor 1 cluster (cluster 5) and the expression levels of *hmgb2b*, *stmn1a*, *nr2e1 sox9b* and *id1*. **(B)** Bright field microscopy images of chromogenic *in situ* hybridization detecting *hmgb2b* on retinal sections of uninjured control animals and at 44 hours post lesion (hpl), 4 days post lesion (dpl) and 6 dpl. The position of the outer nuclear layer (ONL), inner nuclear layer (INL) and ganglion cell layer (GCL) is indicated in the uninjured sample. Scale bar: 30 µm.

Figure 6

A

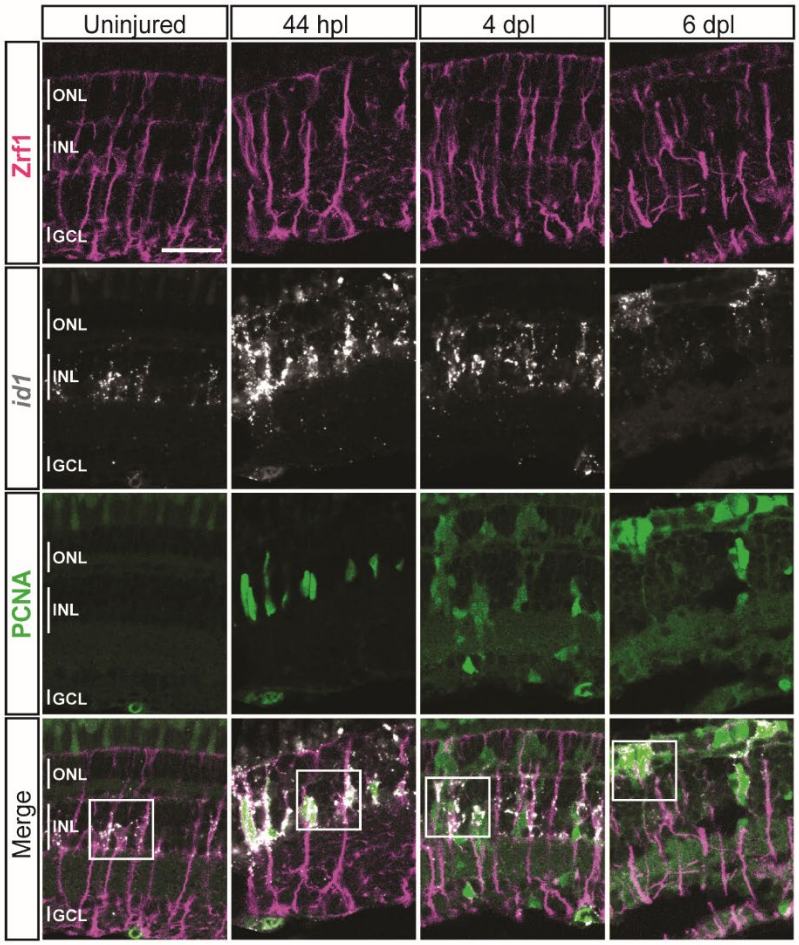
Uninjured
44 hpl
4 dpl
6 dpl
Zrf1
id1
PCNA
Merge
ONL
INL
GCL

B

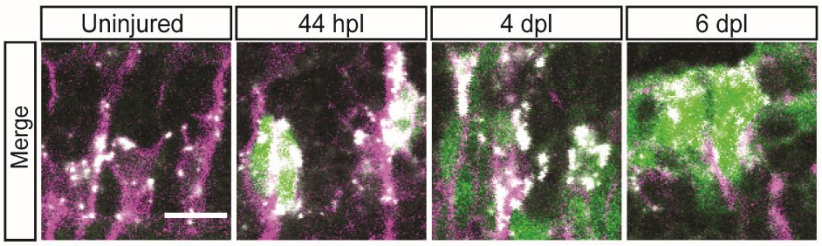
Uninjured
44 hpl
4 dpl
6 dpl
Merge

Figure 6: expression profile of *id1* during retina regeneration. (A) Confocal images of fluorescent *in situ* hybridization for *id1* (grey) and immunohistochemistry detecting Zrf1-positive MG fibers (magenta) and the proliferation marker PCNA (green) on retinal sections of uninjured control animals and at 44 hours post lesion (hpl), 4 and 6 days post lesion (dpl). The position of the outer nuclear layer (ONL), inner nuclear layer (INL) and ganglion cell layer (GCL) is indicated in the uninjured sample. Scale bar: 30 µm. **(B)** Magnification of the areas indicated by the squares 1 and 2 in panel A. Scale bar: 10 µm.

Figure 7

A

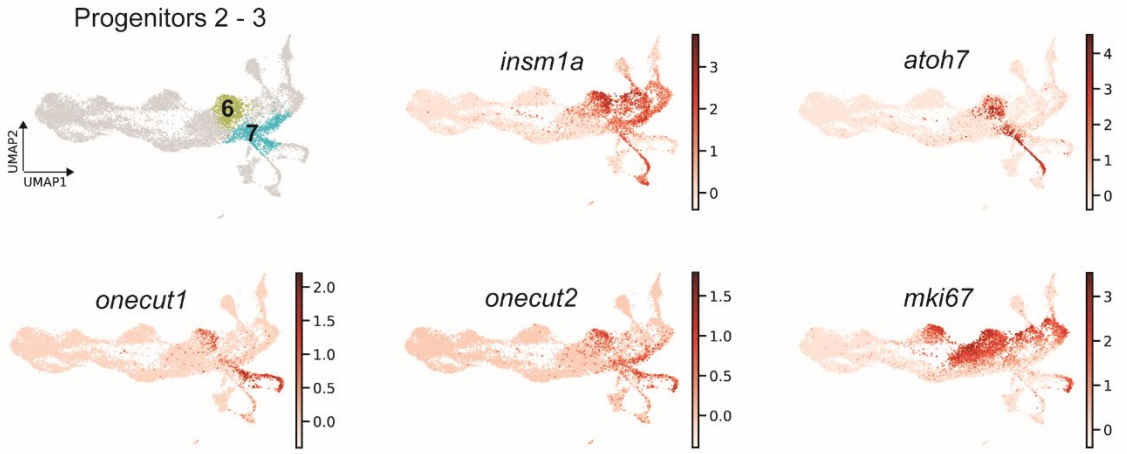
Progenitors 2 - 3
6
7
UMAP2
UMAP1
insm1a
atoh7
onecut1
onecut2
mki67

B

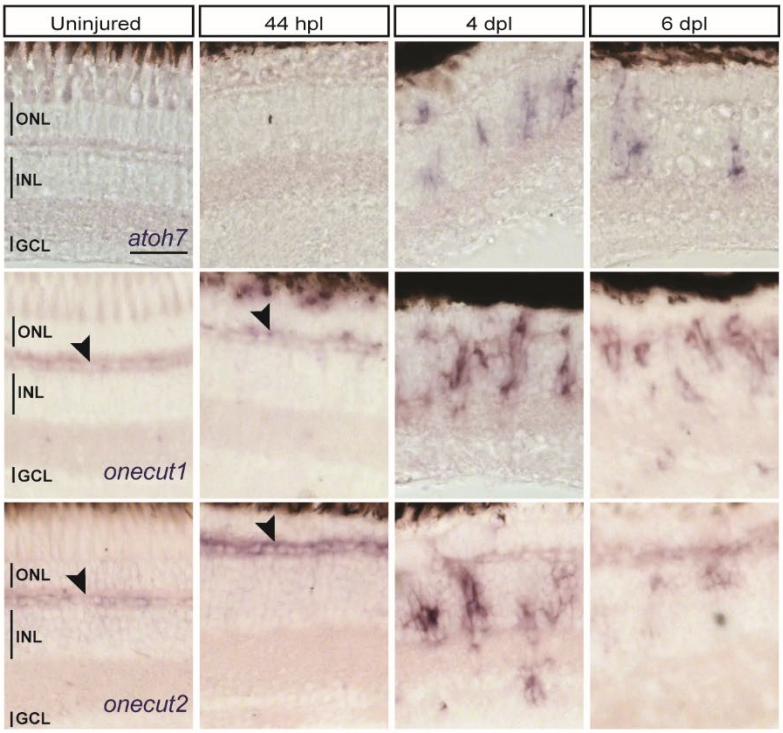
Uninjured
44 hpl
4 dpl
6 dpl
ONL
INL
GCL
atoh7
onecut1
onecut2

Figure 7: scRNAseq identifies two neurogenic progenitor populations in the light-lesioned retina. (A) The two progenitor clusters (cluster 6 and 7) and the relative expression levels of *insm1a*, *atoh7*, *onecut1*, *onecut2* and *mki67*. **(B)** Bright field microscopy images of chromogenic *in situ* hybridization detecting *atoh7*, *onecut1* or *onecut2* on retinal sections of uninjured control animals and at 44 hours post lesion (hpl), 4 days post lesion (dpl) and 6 dpl. The position of the outer nuclear layer (ONL), inner nuclear layer (INL) and ganglion cell layer (GCL) is indicated in the uninjured sample. Scale bar: 30 µm.

Figure 8

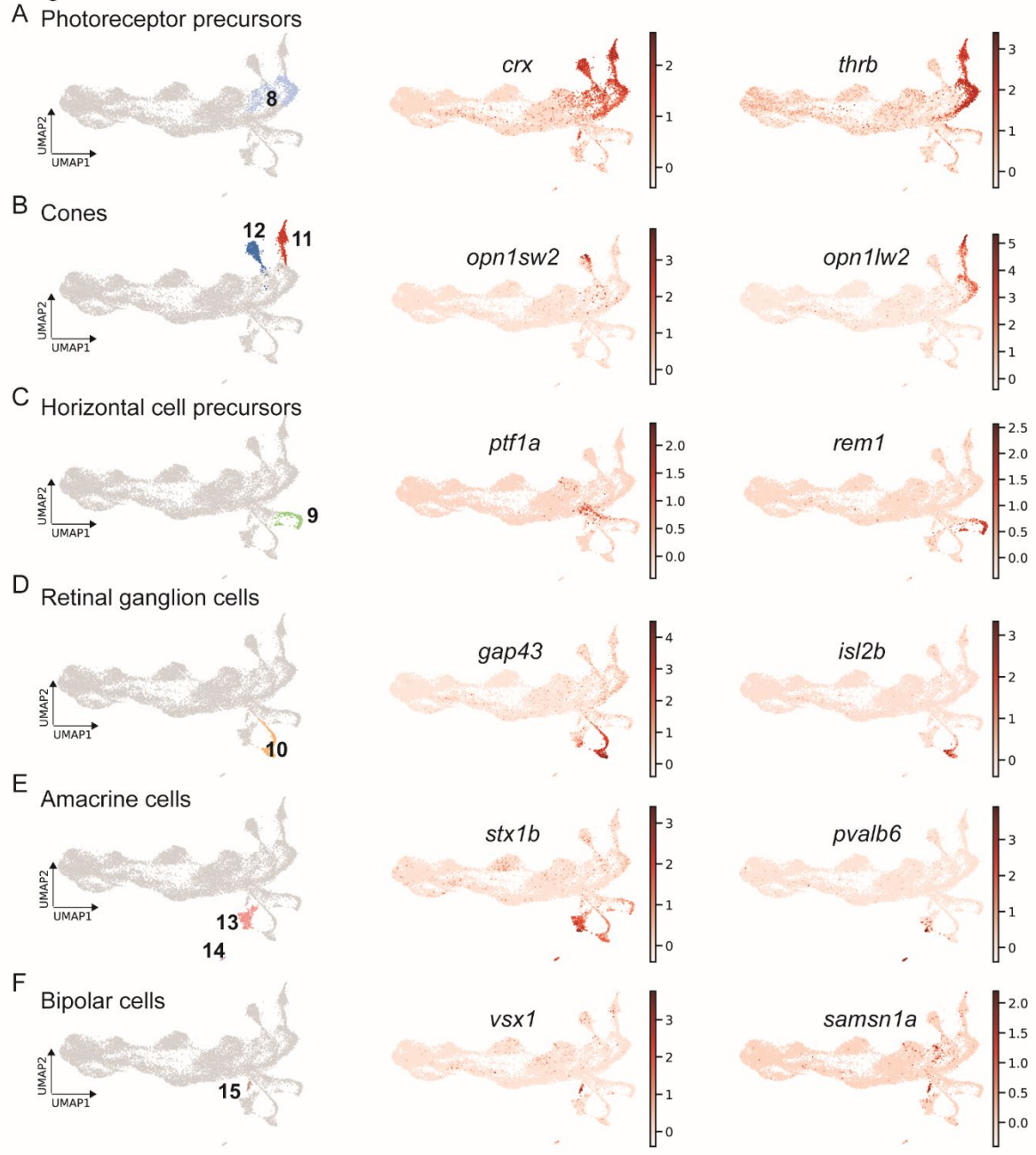
A Photoreceptor precursors
8
crx
thrb
B Cones
12
11
opn1sw2
opn1lw2
C Horizontal cell precursors
9
ptf1a
rem1
D Retinal ganglion cells
10
gap43
isl2b
E Amacrine cells
13
14
stx1b
pvalb6
F Bipolar cells
15
vsx1
samsn1a
UMAP1
UMAP2

Figure 8: scRNAseq identifies fate-restricted progenitors and differentiating progeny in the light-lesioned retina. (A) The photoreceptor precursor cluster (cluster 8) and the expression levels of *crx* and *thrb*. **(B)** The red and blue cone cluster (cluster 11 and 12) and the expression levels of the blue cone marker *opn1sw2* and red cone marker *opn1lw2*. **(C)** The horizontal cell precursor cluster (cluster 9) and the expression levels of *ptf1a* and *rem1*. **(D)** The ganglion cell cluster (cluster 10) and the expression levels of *gap43* and *isl2b*. **(E)** The two amacrine cell clusters (cluster 14 and 15) and the expression levels of *stx1b* and *pvalb6*. **(D)** The bipolar cell cluster (cluster 15) and the expression levels of the known bipolar cell marker *vsx1* and the novel marker *samsn1a*.

Figure 9

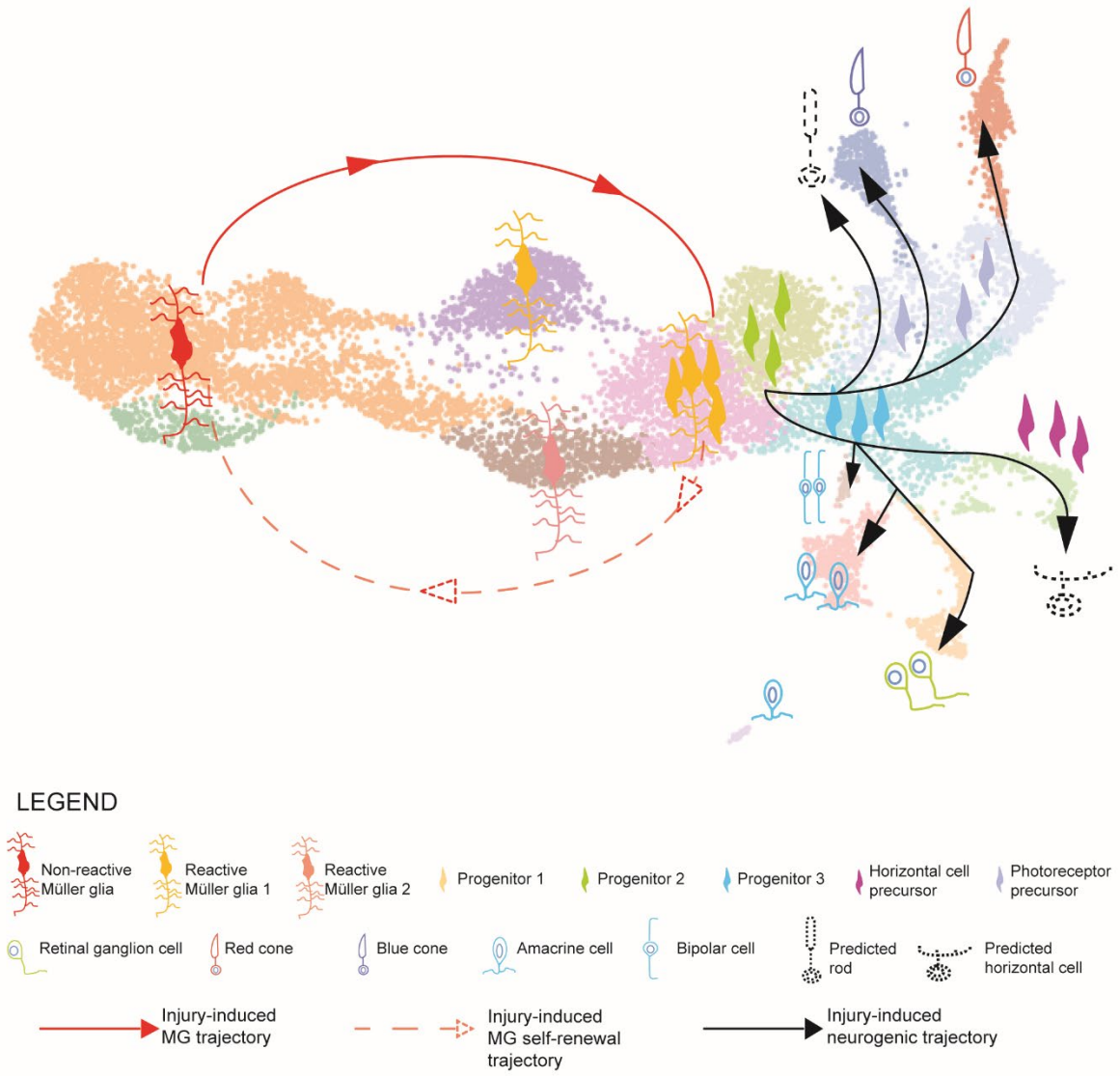
LEGEND
Non-reactive Müller glia
Reactive Müller glia 1
Reactive Müller glia 2
Progenitor 1
Progenitor 2
Progenitor 3
Horizontal cell precursor
Photoreceptor precursor
Retinal ganglion cell
Red cone
Blue cone
Amacrine cell
Bipolar cell
Predicted rod
Predicted horizontal cell
Injury-induced MG trajectory
Injury-induced MG self-renewal trajectory
Injury-induced neurogenic trajectory

Figure 9: model summarizing the cellular events underlying retina regeneration in zebrafish. Upon lesion, non-reactive MG on the left side of the main transcriptional UMAP feed into a hybrid Müller glia/progenitor population via reactive Müller glia (solid red line). Based from this hybrid cell population, we find a Müller glia trajectory reverting to the initial starting point indicating Müller glia self-renewal (dashed red line). Moreover, the hybrid cell population represents the tip of the neurogenic trajectory, resulting in the formation of neuronal precursors and differentiating neurons (solid black lines). Differentiating rods and horizontal cells, which have not been found in the scRNAseq, are indicated with dashed lines and positioned in the predicted location on the main UMAP.